Faculty of Science
Physics and Astronomy

August 5, 2021
Study year 2020-2021

Colliding Muons at the Multi-TeV Energy Frontier

A bachelor's thesis towards the effects of electroweak Bremsstrahlung and reconstruction difficulties in a Muon Collider

Supervisors
Dr. F. Filthaut
Prof. dr. R. Kleiss

Author
Bob Truijen
(s1022573)

Second reader
Dr. M. Wu

Radboud University

Acknowledgements

Throughout the research and writing of this thesis, I have received a great deal of help and support, which shall not go unnamed:

I would first like to thank my supervisors Frank Filthaut and Ronald Kleiss, whose expertise was invaluable in preparing, conducting and evaluating the research. Your help, explanations and feedback brought my knowledge and my work to a higher level.

I would like to acknowledge Rob Verheyen, whose research and work towards the implementation of EW effects in antenna parton showers laid the foundation for this thesis. I also want to thank you for the help, discussions and explanations during my research.

In addition, I would like to thank my friend Olivier, who contributed by improving the use of English in this text and increasing its legibility.

Finally, I would like to thank my parents Joris and Hetty, my sister Maartje, my girlfriend Anne and her parents Els and Charles for the helpful discussions, their wise counsel and sympathetic ear.

Abstract

The aim of this thesis is to explore the effects of the multi-TeV energy regime obtained by a Muon Collider. The research is twofold. Electroweak (EW) Bremsstrahlung is neglected in processes at current colliders. However, *future* colliders operating at the energy frontier might be severely affected by EW Bremsstrahlung. This thesis investigates the effects of said radiation on event-selection procedures of the process $\mu^+\mu^- \to Zh$, where $Z \to \nu\overline{\nu}$ and $h \to b\overline{b}$ in a Muon Collider operating at a centre of mass (CM) energy of 10 TeV. In addition, the difficulties arising in the event-reconstruction of this process are explored. By means of the simulations `MadGraph 5`, `Pythia 8` and `Delphes`, it is shown that the inclusion of EW effects enables the Higgs to transfer momentum to the Z boson, allowing the Z to split into a heavier particle-antiparticle pair. In turn, this leads to the formation of extra jets and consequently a reduction of more than 20% in event-selection efficiency for cuts based on the reconstructed Higgs mass and the difference in pseudorapidity between the jets. Choosing to put b-tagging as the first requirement in the selection procedure might mean elimination of these efficiency reductions. Beyond that, the 10 TeV CM energy is found to cause highly collimated jets, resulting in difficulties in jet reconstruction. Furthermore, the Higgs mass was reconstructed 25 GeV too low and the mass of the Z boson could not be reconstructed at all. The most likely cause is the limited (simulated) detector resolution. Hence, it is necessary to conduct further research towards the feasibility of the required detector resolution at this multi-TeV energy domain.

Summary for the General Public

The Standard Model is the generally accepted theory of particle physics, describing the laws concerning behaviour of and interactions between particles at the smallest length scale. This theory is tested using particle accelerators such as the Large Hadron Collider (LHC) at CERN, where subatomic particles are collided at enormous energies. Such collisions can break the subatomic particles into even smaller pieces; these smallest particles are those the Standard Model makes predictions about.

In 2012, a particle that has been theoretically predicted was discovered at the LHC: the Higgs boson. This boson is essential for the Standard Model; it 'gives mass' to the other particles in the theory. Since this discovery, physicists have been busy investigating as many properties of this Higgs boson as possible. However, the LHC cannot produce enough Higgs bosons to fully unravel the physics behind this particle, so either an LHC upgrade or a new collider is needed.

One consideration for a new collider is the Muon Collider. Muons are elementary particles, whereas protons (the particles being collided at the LHC) are composite particles, i.e. they are built up *from* elementary particles. The energies of the protons at the LHC do not entirely go into the interesting collision between the underlying fundamental particles. There are 'uninteresting' particles that carry away some energy. Colliding elementary particles, however, enables collisions at much higher energies, since all the energy is put in the interesting interaction. Furthermore, there are many fewer uninteresting collisions along with the actual interesting collision, such that the detector obtains much 'cleaner' information. This clean environment together with the high collision energies is perfect for creating and detecting many Higgs bosons and therefore for unravelling the Higgs physics.

However, there might be a catch. The extremely high energies that can be obtained by a Muon Collider could cause the particles in the interaction to start radiating other particles[1] that pollute the environment. This radiation, known as electroweak (EW) Bremsstrahlung, might therefore make it difficult to select the interesting collisions and to properly investigate what happened during the collision. Apart from this EW Bremsstrahlung, other difficulties might arise due to the extremely high collision energy. It is possible that particles are not detected properly due to insufficient detector resolution. As a result, selections for interesting collisions may not work efficiently anymore.

In this thesis, simulations of collisions at a Muon Collider and its detector are used to investigate difficulties concerning the reconstruction of the collisions arising due to the high collision energy. Following this, the effects of EW Bremsstrahlung on the efficiency of selections used to find the interesting collisions for a specific process[2] are investigated.

It has been found that EW effects significantly decrease the efficiency of selection procedures. It is therefore necessary to take the effects of EW Bremsstrahlung into account when creating a selection procedure for interactions at a high-energy Muon Collider. On top of this, it has been found that the particles that are used to identify the collisions (b-quark and $\bar{b}$-quark), travel very near one another. Hence, it is difficult to reconstruct the collision process properly using current reconstruction techniques. Moreover, the masses of the particles that are created directly after a collision (the Higgs and the Z boson) cannot be reconstructed well, most likely due to the aforementioned limited detector resolution.

In conclusion, this thesis has found two important aspects concerning the effects of the extremely high energies that can be obtained by a Muon Collider. Firstly, at energies of this magnitude, EW effects play a significant role in the efficiency of selection procedures. Secondly, in order to properly reconstruct collisions, serious research needs to be conducted towards the feasibility of the required detector resolution.

[1] $W^{\pm}$ and Z bosons.

[2] The process under investigation is $\mu^+\mu^- \to Zh$, where $Z \to \nu\bar{\nu}$ and $h \to b\bar{b}$.

Samenvatting voor Algemeen Publiek (Dutch)

Het Standaard Model is de algemeen geaccepteerde theorie binnen de deeltjesfysica. Het probeert de natuurwetten te beschrijven die subatomaire deeltjes volgen. Deze theorie wordt getest door middel van deeltjesversnellers, zoals de Large Hadron Collider (LHC) bij CERN. In deze versneller worden deeltjes op elkaar gebotst met enorm hoge energieën. Door deze botsing kunnen de subatomaire deeltjes uiteen vallen in hun bouwstenen. Deze bouwstenen zijn de deeltjes waarover het Standaard Model voorspellingen doet.

In 2012 is er een deeltje dat theoretisch was voorspeld door het Standaard Model ontdekt bij de LHC: het Higgs boson. Dit boson is essentieel voor het Standaard Model; het 'geeft massa' aan de andere deeltjes in de theorie. Sinds deze ontdekking zijn fysici druk in de weer om zo veel mogelijk eigenschappen van dit Higgs boson te onderzoeken. De LHC produceert echter niet genoeg Higgs bosonen om de natuurkunde achter dit boson te ontrafelen. Daarom is er óf een upgrade van de LHC óf een nieuwe deeltjesversneller nodig.

Een mogelijke nieuwe versneller is de Muon Collider. Muonen zijn elementaire deeltjes, terwijl protonen (die in de LHC op elkaar worden gebotst) samengestelde deeltjes zijn. Dit betekent dat ze zijn opgebouwd uit kleinere, elementaire, deeltjes. De energieën die de protonen bij de LHC hebben, worden niet volledig in de interessante botsing tussen de onderliggende fundamentele deeltjes gestopt. De 'oninteressante' deeltjes die in de protonen zitten, dragen energie weg. Echter, wanneer er *elementaire* deeltjes op elkaar worden gebotst, wordt álle energie in de interessante botsing gestopt. Hierdoor kunnen er veel hogere botsingsenergieën worden bereikt. Bovendien zijn er heel wat minder oninteressante botsingen tijdens de interessante botsing, waardoor de detector veel 'schonere' informatie krijgt. Deze schone omgeving, samen met de hoge botsingsenergieën, is goed geschikt om veel Higgs bosonen te maken en te detecteren, om zo de fysica achter het Higgs boson te ontrafelen.

Echter, misschien is het niet zo eenvoudig als het lijkt. De enorm hoge botsingsenergieën die bereikt kunnen worden in een Muon Collider zouden ervoor kunnen zorgen dat de deeltjes voor en/of na de botsing andere deeltjes[3] gaan uitstralen die de omgeving 'vervuilen'. Deze straling, die bekend staat als elektro-zwakke (EW)[4] Bremsstrahlung, zou moeilijkheden kunnen veroorzaken in het selecteren van de interessante botsingen en in het onderzoeken van wat er tijdens de botsing precies is gebeurd. Daarbovenop, los van de EW Bremsstrahlung, zouden er andere obstakels kunnen ontstaan door de enorm hoge botsingsenergie. Zo zou het kunnen dat deeltjes niet meer goed gedetecteerd kunnen worden, doordat de detectorresolutie te laag is. Daardoor kan het zijn dat selectieprocedures die worden gebruikt om de interessante botsingen te selecteren niet meer efficiënt werken.

In deze scriptie wordt aan de hand van simulaties van botsingen in een Muon Collider en simulaties van de detector onderzocht wat de effecten zijn van EW Bremsstrahlung op de efficiëntie van selectieprocedures die worden gebruikt om de interessante events te vinden van een specifiek botsingsproces[5]. Daarnaast wordt er onderzocht welke moeilijkheden ontstaan in het reconstrueren van de botsing als gevolg van de enorm hoge botsingsenergie.

Het blijkt dat EW effecten de efficiëntie van selectieprocedures significant verlagen. Het is daarom noodzakelijk om de effecten van EW Bremsstrahlung mee te nemen in het opstellen van een selectieprocedure voor interacties in een Muon Collider. Daarnaast is gevonden dat de deeltjes (b-quark en $\bar{b}$-quark) die worden gebruikt om deze specifieke botsing te identificeren, ontzettend dicht op elkaar liggen. Het is daarom moeilijk om het botsingsproces goed te reconstrueren met huidige reconstructie-methoden. Verder konden de massa's van de deeltjes die direct na de botsing worden gemaakt (het Higgs en het Z boson) niet goed worden gereconstrueerd; dit komt waarschijnlijk door een te lage detectorresolutie.

Samenvattend zijn er in deze scriptie twee belangrijke aspecten gevonden wat betreft de effecten van de enorm hoge botsingsenergieën die bereikt kunnen worden in een Muon Collider. Ten eerste spelen EW effecten een belangrijke rol in de efficiëntie van selectieprocedures. Daarnaast is het, om de interactie goed te kunnen reconstrueren, noodzakelijk dat er uitgebreid onderzoek wordt gedaan naar de haalbaarheid van de vereiste detectorresolutie op deze hoge energieschaal.

[3] $W^{\pm}$ en Z bosonen.

[4] In het Engels is de term 'electroweak Bremsstrahlung', vandaar de afkorting 'EW'.

[5] De interactie die wordt onderzocht is $\mu^+\mu^- \to Zh$, waar $Z \to \nu\bar{\nu}$ en $h \to b\bar{b}$.

Contents

1 Introduction

In the field of physics, our main goal is to discover the fundamental laws of nature; we would like to find the rules that govern the universe. On our human scale, physics can be properly described by classical mechanics: Think of a car accelerating from rest, or a tennis ball hit by Rafael Nadal. However, when we zoom in, all objects appear to be made of tiny building blocks known as atoms. These atoms (and their constituents) seem to follow different laws than we are used to from our human-sized experience. They live in the realm of quantum mechanics; a theory describing how the most fundamental pieces of nature behave and interact.

Atoms, as we learnt in the past century, are composed of smaller constituents: protons, neutrons and electrons. We can go one step further and decompose protons and neutrons into even smaller particles, known as quarks. As far as we are aware now, these quarks are elementary particles, meaning that they cannot be broken down any further. In our current understanding of the quantum world, there exists a handful of such particles, displayed in figure 1. This set of elementary particles, along with the rules by which they behave and interact, constructs a theory known as the Standard Model.

The Standard Model is the generally accepted theory in the field of particle physics. This theory makes predictions that can be tested in particle accelerators. In these machines, particles are accelerated to extremely high energies, to be subsequently collided with each other. The particles shatter into their fundamental building blocks, which undergo all types of interactions. Physicists study what happens during these collisions and thereby test the predictions of the Standard Model.

In 2012, the Standard Model had a large success: the discovery of the Higgs boson. This particle plays an essential role within the theory; it proves the existence of the Higgs field, that accounts for the the masses of the particles in the Standard Model. Since the discovery of the Higgs boson, much effort has been put into determining the characteristics of the particle. However, the Large Hadron Collider (LHC), where the Higgs boson has been discovered, does not produce enough Higgs bosons nor has an adequate resolution to fully investigate the Higgs boson and its features. Therefore, either an upgrade of the LHC or a new collider is needed.

Among other candidates, a proposed new collider is the Muon Collider, colliding muons with antimuons. This collider can reach effective collision energies in the multi-TeV energy domain, which is far beyond the range of the LHC. Furthermore, collisions in the Muon Collider are expected to be 'cleaner' such that they can be more easily reconstructed. These properties make the Muon Collider interesting for creating and detecting many Higgs bosons.

However, there might be a catch. No colliders have yet operated at the multi-TeV energy regime. These enormous energies might cause the particles to radiate $W^{\pm}$ or Z bosons, known as electroweak (EW) Bremsstrahlung. At current colliders, the effects of EW Bremsstrahlung could be neglected because of the 'low' energies of the interacting particles. However, the effects of EW Bremsstrahlung might not be negligible at a Muon Collider. Furthermore, other difficulties might arise due to the multi-TeV collision energies, concerning reconstructions being done by the detector. The detector reconstructs the kinematics of the particles in the collisions. These reconstructions are essential for selecting the interesting collisions from all collisions, of which the majority is uninteresting.

By means of simulations `MadGraph 5`, `Pythia 8` and `Delphes`, this thesis investigates the effects of EW Bremsstrahlung on event-selection procedures[6] of the process $\mu^+\mu^- \to Zh$, where $Z \to \nu\overline{\nu}$ and $h \to b\overline{b}$ in a Muon Collider operating at a centre of mass (CM) energy of 10 TeV. In addition, research is conducted towards the difficulties arising in event-reconstruction of this process.

Chapter 2 serves as detailed background information for the reader and puts forth the research questions and motivation. Chapter 3 is devoted to the difficulties in event-reconstruction. First, the software packages used for the simulations are introduced in paragraph 3.1. Then, in paragraph 3.2 the simulation is validated by comparing theoretical predictions on the kinematics of the Z and Higgs bosons with the results from the simulation. In paragraphs 3.3 and 3.4 respectively reconstructions of the Higgs and Z bosons are investigated. Chapter 4 investigates the effects of the inclusion of EW Bremsstrahlung. In paragraphs 4.2 and 4.3 research is conducted towards the effects of the inclusion of EW Bremsstrahlung on particle reconstructions and in paragraph 4.4 its

[6] In particle physics, a collision is mostly referred to as an 'event'.

effect on the efficiency of event-selection procedures is investigated. The results are summarised in chapter 5. Discussion on the results and ideas for new research are presented in chapter 6.

2 Context

This chapter serves as background information for the reader to understand the research questions and the research carried out in this thesis. Section 2.1 gives an introduction on the theory of the Standard Model and touches physics beyond the Standard Model. Then, in section 2.2 general features of particle accelerators and detectors are put forth. Working towards the research questions, section 2.3 introduces the Muon Collider. Next, two phenomena are explained that are essential for the research questions: Jets (section 2.4) and Bremsstrahlung (section 2.5). Section 2.6 finishes this chapter by putting forth the research questions and motivation.

2.1 Standard Model (and beyond)

The Standard Model is one of the most successful theories within physics and has made many predictions that have been experimentally confirmed. Let us dive deeper into this quantum theory and see what it is made of.

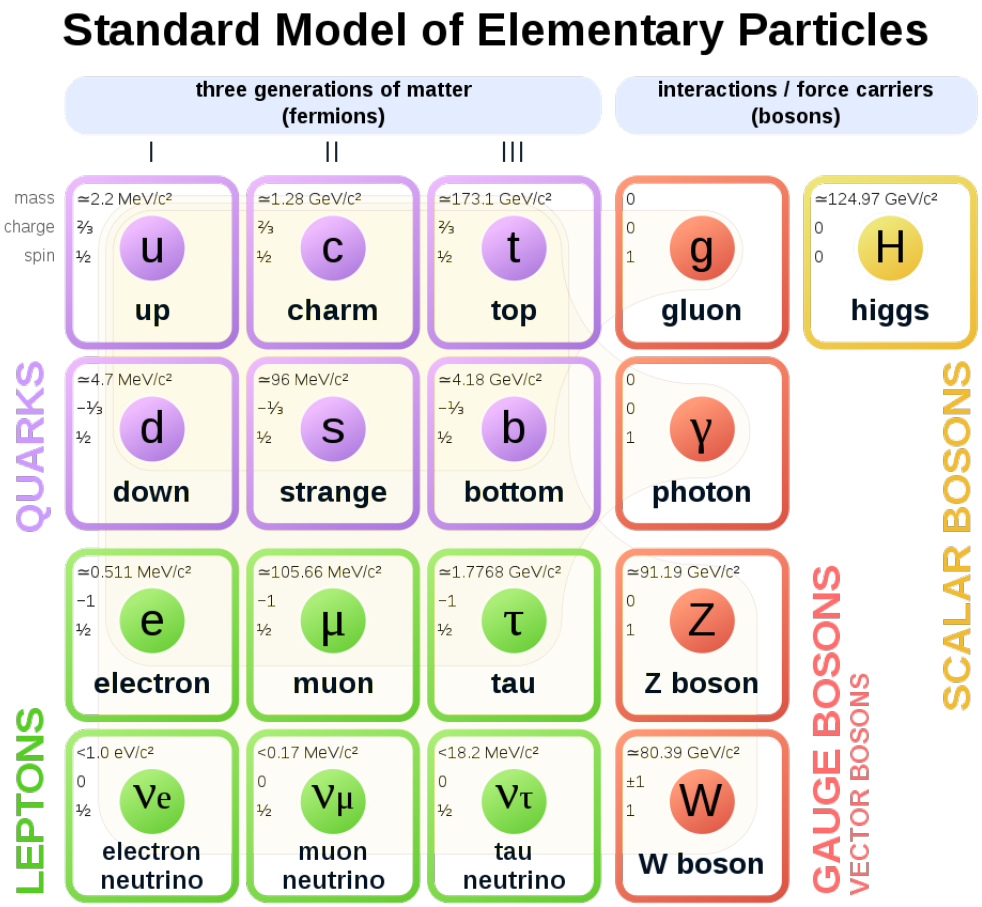

Figure 1: *Elementary particles of the Standard Model. [1]*

Elementary particles As shown in figure 1, the Standard Model contains particles called fermions and bosons. Fermions are the 'matter' particles and can be divided into quarks and leptons. There are six different quark types, known as flavours: up (u), down (d), charm (c), strange (s), top (t) and bottom (b). The up and down quarks have the lowest mass of all quarks and are therefore stable. The other quarks are heavier and rapidly transform (i.e. decay) into their lighter siblings. Quarks have a property called colour, which can be red (r), green (g) or blue (b),

and appear in bound states (combinations of multiple quarks) by which they constitute matter; e.g. protons are built from two up quarks and one down quark (uud), whereas neutrons have the combination udd.

Leptons, the other group of fermions, are also divided into six flavours. Three flavours constitute charged leptons: electron (e^-), muon (μ^-) and tau (τ^-). The other three flavours constitute their corresponding neutral leptons, known as neutrinos: the electron neutrino (ν_e), muon neutrino (ν_μ) and tau neutrino (ν_τ).

As mentioned before, the elementary particle species alongside fermions in the Standard Model are bosons (right part of figure 1). These particles can transmit three of the four fundamental forces of nature: the electromagnetic (EM) force, the strong nuclear force and the weak nuclear force. The fourth fundamental force would be gravity, however, at the scale of elementary particles, gravity is negligible[7]. The EM force is transmitted by photons (γ) and acts on charged particles. The strong nuclear force is mediated by gluons (g) and acts on coloured particles (e.g. quarks). Finally, the weak nuclear force can be carried by the charged W^+ or W^- boson or the neutral Z^0 (or simply Z) boson.

On top of all this, there is a fifth boson: the Higgs boson. This was the last particle in the Standard Model to be experimentally discovered and is in some way responsible for the masses of the other fundamental particles. The more massive a particle is, the stronger it couples to (i.e. interacts with) the Higgs boson.

For each particle in the Standard Model, there is an associated antiparticle. This is a particle with the same properties, but with opposite (colour) charge. For example, the anti-electron (or positron) e^+ has the same mass as the electron, but charge $+e$ (whereas the electron has charge $-e$). Typically, antiparticles are denoted with a bar on top of the corresponding symbol for the particle, e.g. bottom antiquark ($\overline{b}$) or muon antineutrino ($\overline{\nu}_\mu$).

Feynman diagrams The probabilities for interactions between elementary particles can be calculated using the mathematical framework of the Standard Model. One typically calculates the square of the so-called 'matrix element' $|\mathcal{M}|^2$ in order to find such a probability. Richard Feynman realised there is a striking characteristic of the equations one obtains from calculating $|\mathcal{M}|^2$. The terms in the equations can be factorised so that each term can be linked to a visual representation of part of the process. This amazingly creative insight can be best explained by example: Consider the process of electron-muon scattering, $e^-\mu^- \to e^-\mu^-$, in which the electron and muon interact via a photon exchange. Figure 2 shows the Feynman diagram corresponding to this process. The time-axis is drawn horizontally (from left to right) and the space-axis is drawn vertically. The lines are called propagators and represent particles. The points where multiple lines meet represent interaction points and are called vertices; each of these propagators and vertices corresponds to a specific mathematical term[8] [2]:

- Each vertex contributes a factor $ig_e\gamma^\mu$.
- The electron and muon propagators each contribute a factor $\frac{i(\gamma^\mu q_\mu + mc)}{q^2 - m^2c^2}$ with m either the electron or muon mass.
- Furthermore, the photon propagator contributes a factor $\frac{-ig_{\mu\nu}}{q^2}$.

By combining those factors and following the so-called Feynman rules, we obtain an expression for the matrix element:

$$\mathcal{M} = -\frac{g_e^2}{(p_1 - p_3)^2}[\overline{u}^{(s_3)}(p_3)\,\gamma^\mu u^{(s_1)}(p_1)][\overline{u}^{(s_4)}(p_4)\,\gamma_\mu u^{(s_2)}(p_2)] \tag{1}$$

[7] As an example to show the weakness of gravity compared to the strength of the EM force, do the following thought experiment: Imagine lifting a paperclip from the table with a little magnet. Then, zoom out so that you can see the entire Earth. The strength of the magnet (i.e. EM force) easily opposes the strength of entire Earth's gravity pulling on the paperclip!

[8] The meaning of all the terms in these equations are beyond the scope of this thesis and will not be further explained. The equations are shown solely to give a feeling for the power of Feynman diagrams.

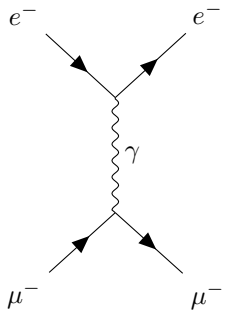

Figure 2: *Feynman diagram for electron-muon scattering,* $e^-\mu^- \to e^-\mu^-$.

From this matrix element, we can directly determine the probability of this specific process. So, just by drawing a process using a Feynman diagram (and following the Feynman rules) we immediately obtain an expression for its probability!

Predictions A handful of successful predictions[9] by the Standard Model are:

- The magnetic moment of the electron and positron. [3]
- The existence of a 125 GeV scalar boson with even parity, zero electric charge and zero spin, called the Higgs boson. [4]
- The coupling strengths of the Higgs boson with other particles. [4]
- The probability of the scattering process $e^+p \to e^+X$ at high x and high Q^2, where X represents the final-state hadronic system. [5]

These predictions have been put to the test in particle accelerators where particles are collided at high energies.

Beyond the Standard Model As glamorous and celebrated as it is, the Standard Model does not account for everything we observe in nature. A few examples:

- The stars at the edges of rotating spiral galaxies move at higher speeds than expected based on the mass we observe in these galaxies [6, 7]. At these speeds, the outer stars should just be ejected from their orbits. However, since this is not the case, there must be mass in the galaxies we cannot see. This 'invisible' mass is known as dark matter. Another observation supporting the existence of dark matter comes from gravitational lensing [6]: According to Einstein's theory of general relativity, massive objects curve spacetime. Light rays follow this curvature and therefore appear to travel on a path that is not 'straight'[10], but deflected. Strangely, we observe this phenomenon at locations where there is no massive object to be seen.
- The universe undergoes an accelerated expansion. This observation has led to the concept of dark energy; energy with a negative pressure. This dark energy accounts for approximately 68.9% of the total cosmic energy density [8].
- The matter-antimatter asymmetry problem: Almost everything we observe consists of matter. Hence the question: where is all the antimatter? [9].

Since the Standard Model does not explain all observations, there is a need for other models that do account for these phenomena: models beyond the Standard Model.

[9] The predictions of the Standard Model are an interplay between theory and experiment. Experimental input (such as measurements of the masses of fermions) is needed to make concrete theoretical predictions (e.g. the branching ratios of the Higgs boson).

[10] Of course, the validity of this statement depends on the definition of 'straight'.

Figure 3: *Aerial view of the Large Hadron Collider at CERN. [10]*

2.2 Particle accelerator & detector

The Standard Model (and other models) can be tested in particle accelerators. In order to properly explain what typically happens in a particle accelerator, let us consider the example of the Large Hadron Collider (LHC) at CERN, Geneva, Switzerland (see figure 3).

Particle accelerator In the LHC, protons are accelerated to an energy[11] of 7 TeV [11] in two large circular tubes. One tube is designed for clockwise acceleration and the other for anti-clockwise acceleration. Once the protons have obtained sufficient energies, they are collided head-on. In these collisions all kinds of processes happen: the fundamental particles within the protons interact with one another, leading to creation of new particles, annihilation of other particles and many subsequent decays. There is a detector in place around the collision point to detect the resulting particles from said collision.

Detector The LHC features a detector named ATLAS (see figure 4). It consists of different parts, each of which can detect different particle properties. The first (most inner) part is the tracker. Here, charged particles are deflected due to a strong magnetic field. The paths of the particles are tracked, giving information about their charge (by the direction of deflection) and momentum (by degree of curvature). The next part is the electromagnetic calorimeter. Particles that interact electromagnetically deposit (some of) their energy to this part of the detector. Together with the tracker, this facilitates the detection of electrons, positrons and photons. Moving on, there is the hadronic calorimeter. Particles that interact via the strong force leave a trace in this part of the detector by depositing (some of) their energy to the material of the calorimeter. This allows detection of hadronic jets (see section 2.4). The outer-most parts of the detector are the muon chambers. These are combinations of trackers and calorimeters that interact with muons.

Figure 5 shows a single event (i.e. a single proton-proton collision) detected by ATLAS. Using data from the detector, physicists can deduce and reconstruct what processes took place during

[11] At this energy, protons travel at 99.999% of the speed of light.

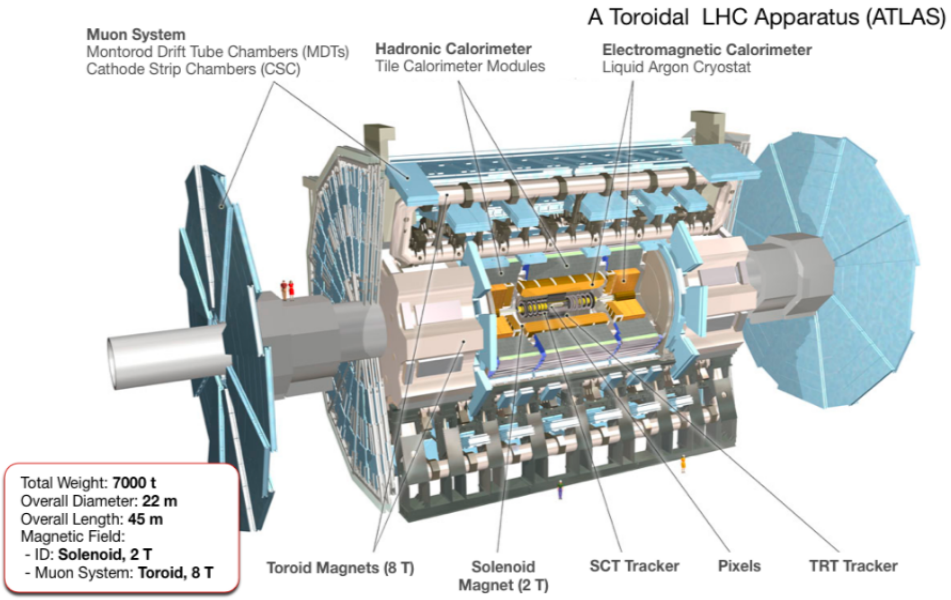

Figure 4: *Schematic overview of the ATLAS detector. [12]*

the event. This is then used to verify the Standard Model.

An important note is that not all particles are detected by the detector. Neutrinos interact very weakly with other particles and are therefore not picked up. The same goes for dark matter. However, the inability to directly measure these particles does not mean that we do not know anything about them. We know that the protons are collided head-on, so initially there is no momentum perpendicular to the proton beam; i.e. there is no transverse momentum. During the event, momentum is conserved, so transverse momentum must still be zero afterwards. So, in summing all the measured transverse momentum vectors, $\sum_i \boldsymbol{p}_{T,i}$, we know that the transverse momentum vector of the particles that evaded the detector must be $-\sum_i \boldsymbol{p}_{T,i}$. In the Standard Model, this 'missing transverse momentum' is usually assigned to neutrinos (since it has no dark matter particles).

Luminosity Each particle collider has a crucial property called luminosity; an indirect measure of the number of collisions. Luminosity is defined as:

$$\mathcal{L} = \frac{1}{\sigma}\frac{dN}{dt} \tag{2}$$

with $\mathcal{L}$ the luminosity (in $\mathrm{b}^{-1}\mathrm{s}^{-1}$), σ the cross section (in b)[12] and dN/dt the event rate (in events s^{-1}).

In practice, *integrated* luminosity is often used. This is the luminosity integrated over the data taking period:

$$\mathcal{L}_{int} = \int \mathcal{L}\, dt \tag{3}$$

Knowing the cross section of a process, one can calculate the number of events to be expected for that specific process over the total data taking period:

$$N = \mathcal{L}_{int}\, \sigma \tag{4}$$

[12]Barn (b) is a measure of area, often used for cross sections. 1 b is defined as 10^{-28} m^2.

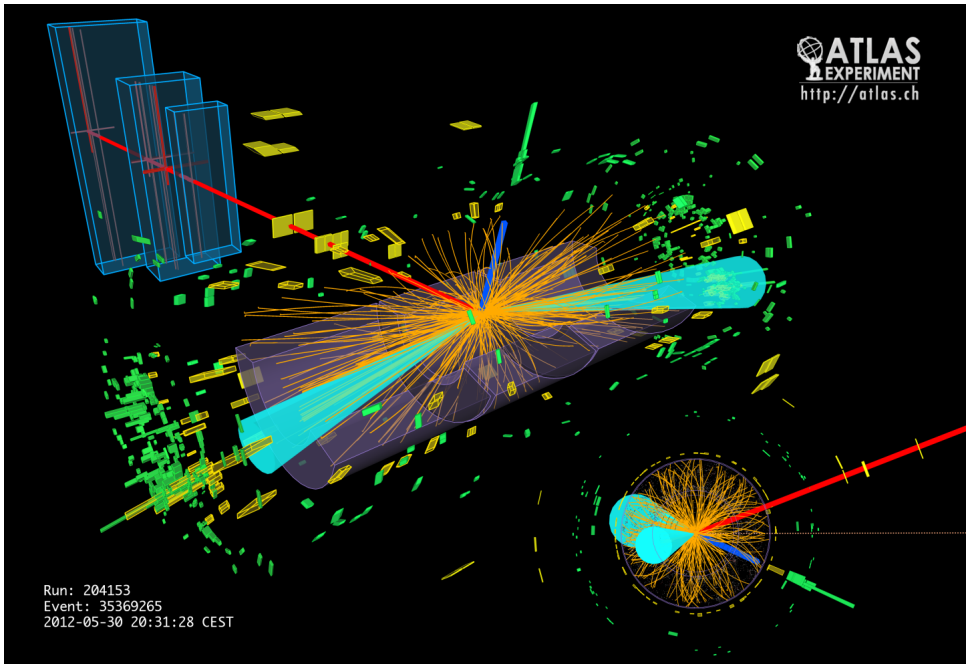

Figure 5: *Higgs candidate decaying to 2 tau leptons in the ATLAS detector. [13]*

2.3 Muon Collider

Since the discovery of the Higgs boson in 2012 [14, 15], physicists have been busy trying to determine as many properties of the Higgs as possible. E.g. the mass of the Higgs boson, its branching ratios and the process of Higgs self-coupling. Although the LHC was the first collider at which the Higgs boson was detected, it does not produce enough Higgs bosons nor does it have a sufficient resolution to fully unravel the physics of the Higgs. Therefore, either an upgrade at the LHC or a new collider is required.

Furthermore, as was already touched upon in the discussion of section 2.1: The Standard Model lacks explanation of certain phenomena. Theories beyond the Standard Model (BSM) are needed to explain these phenomena. So, it is crucial to have colliders that can probe 'new physics' and thereby test BSM theories. The LHC may have the capabilities to probe new physics, but a higher-energy collider would be required to properly sort out the physics BSM possibly detected at the LHC [16, 17].

Different colliders have been proposed that operate at the energy frontier and/or have the capability of probing the physics behind the Higgs boson, to name a few: an electron-positron collider, either circular (FCC-ee, CEPC) or linear (CLIC, ILC), a proton-proton collider (FCC-pp) at higher energies than the LHC, and a circular Muon Collider, colliding muons (μ^-) with antimuons (μ^+) [18, 19, 17]. The Muon Collider, although being relatively new to this list, is a serious candidate. The main advantage of a Muon Collider over an electron-positron collider is the suppression of synchroton radiation due to the high muon mass. Compared to proton-proton colliders the Muon Collider has the benefit of colliding elementary particles rather than composite ones. The following paragraphs elaborate on these and other aspects of the Muon Collider.

Colliding elementary particles The LHC collides protons, which are composed of multiple quarks. Hence, the energy put into the actual collision between the underlying fundamental particles is lower than the total centre of mass energy carried by the protons. After all, the individual quarks each carry only part of the proton's momentum. Particle accelerators that collide elementary particles (such as the Muon Collider) therefore need much less energy to obtain the same effective collision energy. To quantify this difference: a 14 TeV Muon Collider would have a similar effective energy to a 100 TeV hadron collider [17]. This characteristic feature of lepton colliders serves the need for effective collisions in the TeV range.

Furthermore, colliding fundamental particles makes events a lot 'cleaner' compared to events in a hadron collider [20].

Synchrotron radiation One of the great advantages of a Muon Collider over other circular lepton colliders is the suppression of synchrotron radiation. Charged particles that are accelerated radially (which is the case for circular colliders) can emit electromagnetic radiation. For particles traveling at relativistic speeds, this radiation is known as synchrotron radiation. It can be a real bottleneck for particle accelerators, limiting the energy to which particles can be accelerated [21]. The power of synchrotron radiation is inversely proportional to m^4 where m is the mass of the accelerated particle [22]. Since the muon is approximately 200 times heavier than the electron [23], it emits $\sim 10^9$ times less synchroton radiation in a circular collider than electrons or positrons would. Therefore, muons can be accelerated to multi-TeV energies without experiencing severe synchrotron radiation [21].

Integrated luminosity Assuming an operating period of five years and a centre of mass energy of 10 TeV, the integrated luminosity of the Muon Collider is estimated to be 10 ab^{-1} [17].

Muon source There are two main proposed muon sources: proton-driven and positron-driven sources [16, 17]:

- *Proton-driven source:*
  A high-power proton beam is collided with a target of heavy material. In this process, pions[13] are created, which subsequently decay into (anti)muons. These (anti)muons have a large phase space, so in order to make a proper beam they need to be cooled down. Since muons have a lifetime of only $2.2 \cdot 10^{-6}$ s [23], they then need to be rapidly accelerated to prevent them from decaying into electrons or positrons. When the beam is well-prepared, it is injected into the collider ring.

- *Positron-driven source:*
  Muons and antimuons are created by letting a positron beam annihilate with electrons in a target. The energy of the beam is such that the (anti)muons end up nearly at rest in the centre of mass frame. Furthermore, the (anti)muons are created with a significant Lorentz boost ($\gamma \sim 200$) so that they are well-collimated to a narrow beam. Consequently, the (anti)muons need not be cooled down for reduction of their phase space.

Both of these ideas have important technical difficulties that should be mentioned. For the proton-driven source, the main drawback is the large phase space of the created (anti)muons [16]. The (anti)muons need to be confined to a phase space that is acceptable for the collider. This process needs to happen fast, such that the (anti)muons can subsequently be accelerated to prevent them from decaying. The main difficulty for the positron-driven source is the small muon production cross section of maximally 1 μb [16]. Hence, a very high positron flux should be created to obtain sufficient (anti)muons [20].

Testing (Beyond) the Standard Model The main objective for the Muon Collider would be to further investigate the Higgs boson and its coupling properties. A Muon Collider could more precisely measure the Higgs coupling to fermions and vector bosons than the LHC. More importantly, the trilinear and quadrilinear Higgs self-couplings could be measured due to the plentiful production of double and triple Higgs bosons [24]. Furthermore, since it operates at the high energy frontier, a Muon Collider could directly and indirectly probe new physics [25] beyond the Standard Model.

[13] Pions are mesons, i.e. a bound state of quark-antiquark. The positively charged pion, π^+, is composed of $u\bar{d}$, whereas the negatively charged pion, π^-, is composed of $d\bar{u}$.

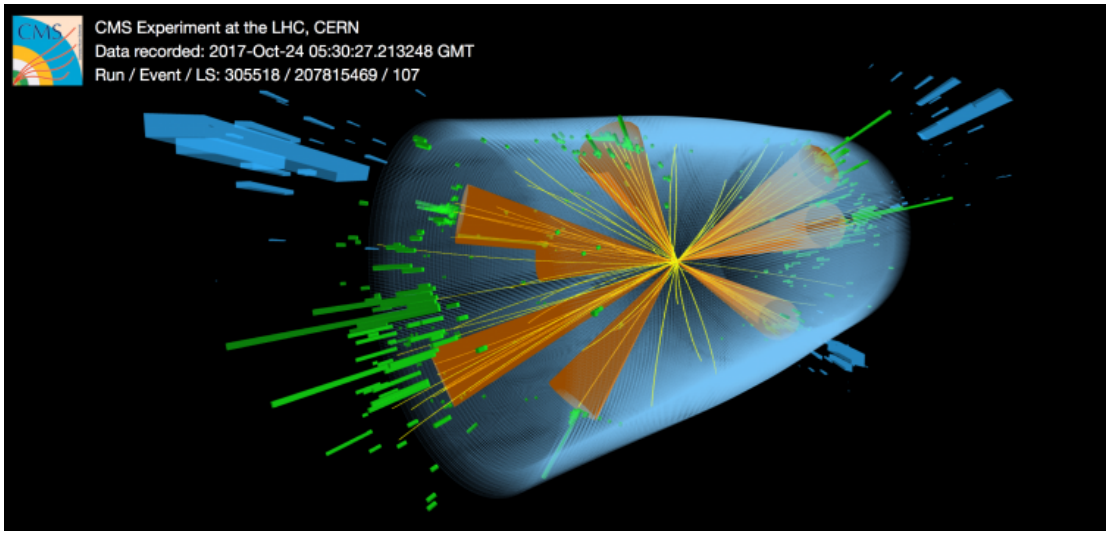

Figure 6: *Collision detected by CMS where; likely resulting in the production of a top-antitop and a bottom-antibottom pair. [26]*

2.4 Jets

Confinement The strong interaction has an important property: its potential $V(r)$ grows with distance r. This means that the further coloured particles are separated, the higher the potential between these particles will be. When the coloured particles are separated sufficiently far, it becomes energetically favourable to produce a new quark-antiquark pair between the original coloured particles. This process repeats until there is not enough energy left to produce another pair. At this stage, pairs (and triplets) of (anti)quarks are pulled together to form respectively mesons and baryons. This property of the strong nuclear force results in a phenomenon called (colour) confinement: coloured particles cannot exist individually in nature, but only appear in bound states called hadrons, which are a colour singlet (i.e. a combination of red, green and blue or colour-anticolour, e.g. red-antired).

Consequently, when a quark-antiquark pair created in a collision is driven apart, the resulting detector image looks like figure 6: Large cone-shaped bundles of hadrons are detected. These hadronic cones are known as jets.

Jet reconstruction Actually, figure 6 shows the *reconstruction* of the collision process, not the direct measurement. As explained in section 2.2, the detector measures particles in the tracker, the EM calorimeter, the hadronic calorimeter and the muon chambers. The hadronic particles in a jet deposit most of their energy to the hadronic calorimeter. However, by mere detection of hadronic particles, the detector does not know which particles belong to a jet and which do not. That is where jet reconstruction algorithms come into play. These algorithms are used to deduce which particles belong to which jet (if one at all).

There are two types of jet reconstruction algorithms: cone algorithms and sequential clustering algorithms [27]. Cone algorithms use the fact that particles in a jet appear in a conical region and that therefore the particles can be selected based on their position in (η,ϕ)-space. Pseudorapidity, η, is a quantity often used in collider physics. It is defined as $\eta = -\ln[\tan(\theta/2)]$ and is a measure of the angle relative to the beam axis. This definition was established with the rise of hadron colliders. The partons within hadrons that collide typically do not have exactly opposite momentum, so the particles created from such a collision often experience a longitudinal boost. The difference in pseudorapidity, $\Delta\eta$, is Lorentz invariant, so that it is independent from any movement of the centre of mass. This makes η a more convenient quantity than θ. At lepton colliders the centre of mass is, however, at rest, so there is no need for such a Lorentz invariant quantity.

In contrast to cone algorithms, sequential clustering algorithms rely on particles within jets having little difference in transverse momentum. So, these algorithms instead select particles based

on their position in momentum-space. The reconstruction algorithm that will be used in this thesis is a sequential clustering algorithm named 'Valencia'. Let us have a look how the algorithm works:

Valencia [28] uses an inter-particle distance variable d_{ij} defined as follows:

$$d_{ij} = \min\left(E_i^{2\beta}, E_j^{2\beta}\right) \frac{1-\cos\theta_{ij}}{R^2} \tag{5}$$

where E_i and E_j are the energies of particles i and j, θ_{ij} is the angle between the two particles, R is the radius parameter that defines the maximum area of the jet and β is a real parameter that influences the significance of particle properties in the clustering process. For example, $\beta = 1$ ensures clustering starts with soft, i.e. low energetic particles [29] (since $d_{ij} \propto \min\left(E_i^{2\beta}, E_j^{2\beta}\right)$), whereas $\beta = -1$ ensures clustering begins around hard particles. $\beta = 0$ would cluster solely based on the angle θ_{ij}. Additionally, a distance variable d_{iB} is used:

$$d_{iB} = p_{T,i}^{2\beta} \tag{6}$$

where d_{iB} is the distance in momentum-space between the particle and the beam-axis [27] and $p_{T,i}$ is the transverse momentum of particle i.

After making a list of all d_{ij} and d_{iB}, the Valencia algorithm finds the minimum value. If d_{ij} is the minimum, the particles i and j are combined into one particle by summing their four-momenta. This combined particle is added to the list and the particles i and j are removed from the list. If d_{iB} is the minimum, particle i is labeled as a final jet and is removed from the list. This process is repeated until either the required amount of jets is found (i.e. exclusive clustering), or until all particles are assigned to a jet (i.e. inclusive clustering) [27].

2.5 Bremsstrahlung

Charged particles that are accelerated or decelerated can radiate electromagnetic radiation, i.e. photons. This phenomenon is called Bremsstrahlung (see figure 7). This concept originates from nuclear physics, but has migrated to the field of high energy physics. Synchrotron radiation, as mentioned in section 2.3, is an example of Bremsstrahlung. Bremsstrahlung is, however, not limited to electromagnetic radiation. Particles that are accelerated or decelerated can radiate any type of bosons to which it can couple. So not only photons, but also gluons, or even $W^\pm$ or Z bosons. Note that photons and gluons are massless, whereas $W^\pm$ and Z bosons are massive bosons. Consequently, a requirement for the radiation of these weak bosons (which is called electroweak (EW) Bremsstrahlung) is that the energy of the accelerated or decelerated particle is sufficiently high. The term Bremsstrahlung is generally reserved for radiation of particles that requires much less energy than the CM energy, so that these particles can be 'easily' radiated.

2.6 Research question and motivation

At the time of writing, electroweak Bremsstrahlung is often neglected in calculations and event-selection procedures concerning LHC experiments. This is justified by the fact that the effective collision energies at the LHC (a few TeV at most) are sufficiently low that the creation of $W^\pm$ or Z bosons requires a large part of the available energy. Therefore, the creation of EW bosons should not be seen as mere radiation, but rather as an important part of the interaction.

Looking at the parton density function (PDF) of protons (figure 8), we see that the probability of finding a parton with fraction x of the proton's total momentum[14] decreases rapidly as x increases. Note that the vertical axis plots the parton density function *times* x. Hence, the actual density functions decay much faster than the figure shows. For a particle (either before or after the collision) to be able to radiate a $W^\pm$ or Z boson, it must have at least enough energy to create such a boson, i.e. ~ 100 GeV. Since this energy comes from the interacting partons within the protons, these partons together must carry ~ 100 GeV.

Suppose that the LHC operates at a CM energy of 14 TeV, then each proton carries approximately 7 TeV. Consequently, a momentum fraction of at least $x \sim \frac{50}{7000} \approx 7.1 \cdot 10^{-3}$ would be

[14] The probability of finding a parton with $a \leq x \leq b$ is obtained by integrating the density function of the parton from a to b.

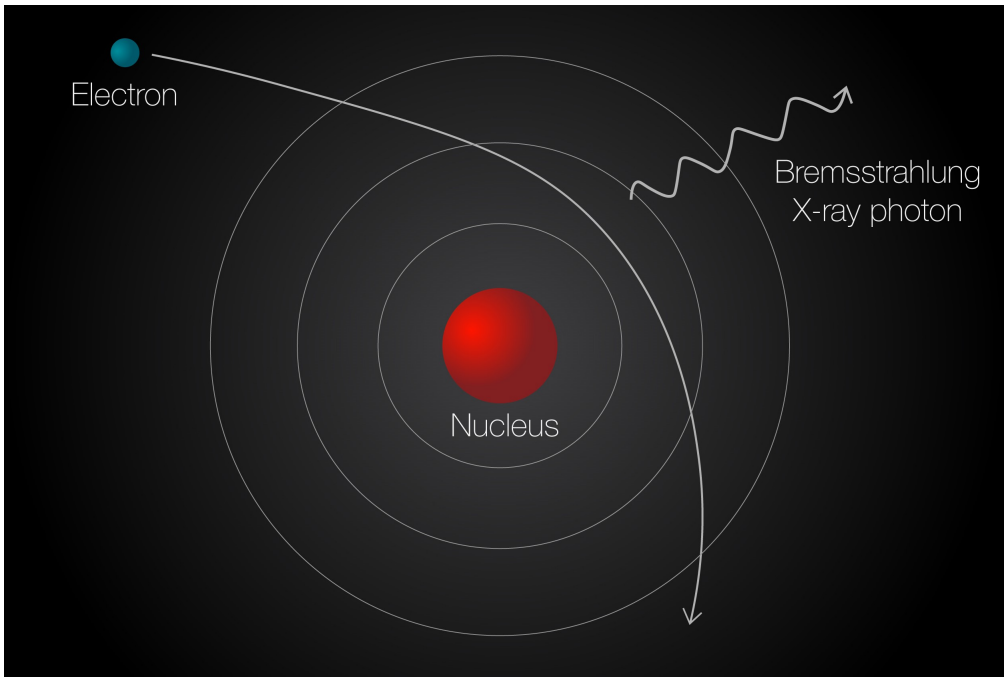

Figure 7: *Electromagnetic Bremsstrahlung produced by a high energetic electron, deflected by a nucleus. [30]*

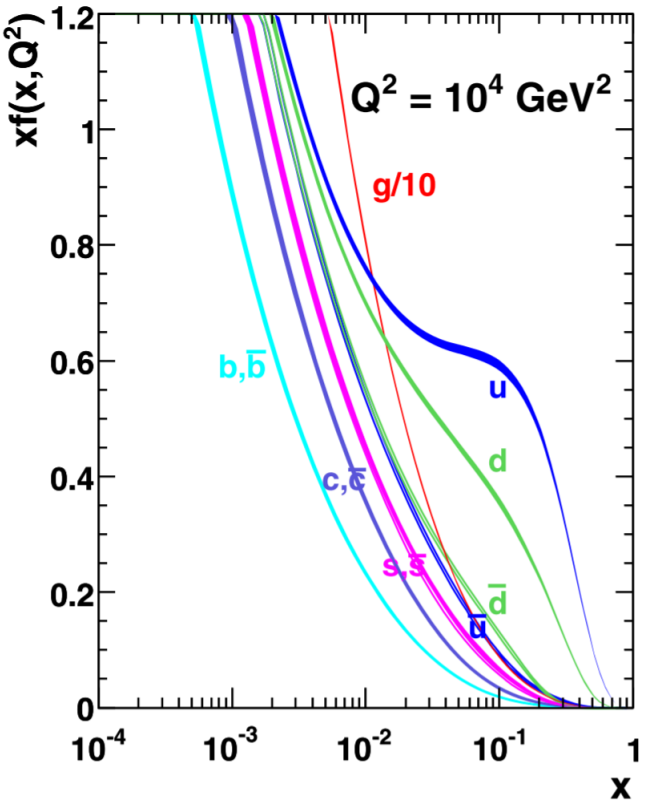

Figure 8: *Momentum fraction x times the parton density function $f(x, Q)$ of the proton versus momentum fraction x for $Q^2 = 10$ GeV^2 [31], where Q is the transferred momentum. Note that the horizontal axis has a logarithmic scale and the vertical axis plots the PDF times x. Hence we can see that $f(x, Q)$ very rapidly decreases with increasing x.*

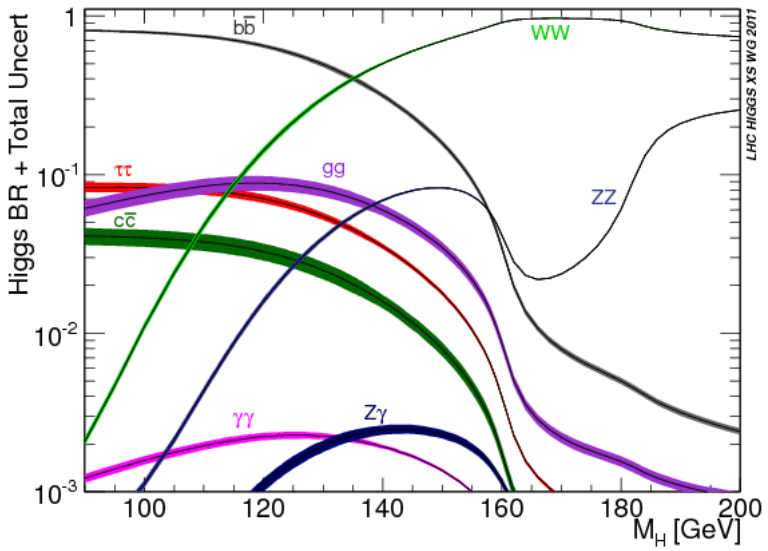

Figure 9: *Higgs decay branching ratios as a function of Higgs mass. [32, 33]*

required[15]. Looking at figure 8, again noting that the vertical axis plots the density function *times* x and realising that the density functions rise even further for $x < 10^{-4}$, we see that by far most of the area under the density functions appears in the region $x < 7.1 \cdot 10^{-3}$. Hence, the probability of finding a parton with $x \geq 7.1 \cdot 10^{-3}$ is very small. So, at the effective collision energies obtained at the LHC, EW Bremsstrahlung occurs very rarely and is negligible.

However, there is no experience whatsoever with the influence of EW Bremsstrahlung at the multiple TeV energy regime of a Muon Collider. In such a collider, effective collision energies of 10 TeV could be obtained, completely changing the rules of the game. Perhaps at these energies EW Bremsstrahlung will play an important role in detecting and selecting events.

In order to get a thorough understanding of the possibilities of a Muon Collider, it is therefore necessary to investigate the effects of EW Bremsstrahlung on the efficiency of event-selection procedures at this higher-energy regime.

As discussed earlier, the aim of a Muon Collider is the detection of Higgs physics. The dominant decay of the Higgs boson is $h \to b\bar{b}$ (see figure 9). This decay leads to the formation of two jets. Phenomenological studies need to investigate whether these jets can still be properly reconstructed at the energy regime of a Muon Collider.

Therefore, this thesis investigates the following two research questions:

1. In a hypothetical Muon Collider operating at a centre of mass energy of 10 TeV, what is the influence of electroweak Bremsstrahlung on the efficiency of event-selection procedures concerning the process $\mu^+\mu^- \to Zh$, where $Z \to \nu\overline{\nu}$ and $h \to b\bar{b}$?

2. What difficulties, if any, occur in the Muon Collider Detector reconstruction of the process $\mu^+\mu^- \to Zh$, where $Z \to \nu\overline{\nu}$ and $h \to b\bar{b}$ at a centre of mass energy of 10 TeV?

There are multiple reasons for investigating this specific process:

1. The neutrinos into which the Z boson decays cannot be detected. Consequently, any signal that does not originate from the Higgs boson nor from the (anti)muon beam must originate from the Z boson[16]. Therefore, any EW Bremsstrahlung originating from the Z boson or

[15] Here, it is assumed that both interacting partons carry 50 GeV and we look only at the probability of a single parton with this energy.

[16] The (anti)muons in the beam can decay before reaching the collision point, leading to the presence of electrons or positrons and (anti)neutrinos that could potentially interfere with the event. Furthermore, the (anti)muons in the beam could radiate photons or weak bosons, i.e. initial state radiation (ISR). However, since the (anti)muons in the beam have an energy of 5 TeV, these decay products or radiated bosons are highly collimated in the beam direction and can therefore easily be differentiated from any signal originating from the Z boson.

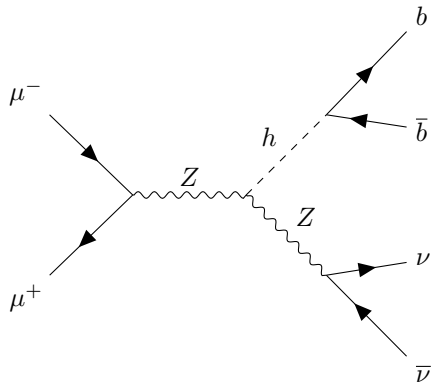

Figure 10: *Feynman diagram of the interaction process to be investigated in this thesis.*

from its daughter neutrinos can be easily identified.

2. With a branching ratio of 0.582, $h \to b\bar{b}$ is the decay of the Higgs boson with the greatest probability [23]. Hence, this is the most natural choice for the Higgs decay.

3. $h \to b\bar{b}$ is a process in which jets are formed. It is interesting to see whether the jets can still be properly reconstructed at the energies in a Muon Collider, i.e. 10 TeV.

4. This process occurs approximately 203 times during the lifetime of the Muon Collider (see appendix A), such that results could be obtained that are statistically interesting. Higgs self-coupling interactions were also considered, but these processes would take place only approximately 12 times during the lifetime of the Muon Collider (see appendix A); so rarely that it does not matter whether or not EW Bremsstrahlung has an effect, since the statistics are too low to investigate the process.

3 Simulation: Event-Reconstruction

3.1 Software

The research questions are investigated using two simulations: one with EW Bremsstrahlung and one without EW Bremsstrahlung. Each simulation consists of three different pieces of software[17] which are run consecutively: `MadGraph 5`, `Pythia 8` and `Delphes`.

MadGraph `MadGraph 5` [34] is a Monte Carlo simulation. As input, it takes the specific process to generate, the centre of mass energy at which the initial particles should collide, and the number of events to be generated. Then, `MadGraph 5` calculates the cross section for the requested process and outputs the four-momenta of the generated particles.

In this thesis, the process $\mu^+\mu^- \to Zh$, with $h \to b\bar{b}$ and $Z \to \nu\overline{\nu}$ was generated at a centre of mass energy of 10 TeV (see figure 10); 10,000 events were generated.

Pythia These four-momenta of the generated particles are then put into the second part of the simulation: `Pythia 8` [35]. This is another piece of Monte Carlo software that calculates the decay of the generated particles and generates the entire hadronisation process, ensuring that all particles with a colour charge end up in a colour singlet state. `Pythia 8` returns the four-momenta of all particles in the event, ranging from the initial muons to all final-state particles.

Recently, the version series `Pythia 8.3` was released. As a result from the PhD research by R. Verheyen [36] this is the first series in which the phenomenon of EW Bremsstrahlung is taken into account, allowing the user to manually enable/disable the EW Bremsstrahlung. This feature is exploited in this thesis by comparing the data resulting from the simulation with EW Bremsstrahlung *enabled*[18] and with EW Bremsstrahlung *disabled*[19].

Delphes Next, the four-momenta from `Pythia 8` are given to `Delphes` [37], the final part of the simulation. `Delphes` simulates the detector; in this case the Muon Collider Detector. It yields the data that an actual detector would observe: tracks from the charged particles in the tracker and 'towers' from energy deposits to the calorimeter.

`Delphes` needs a so-called `Delphes` card, containing all parameters that define the detector. That is to say, the size of the tracker system, the size of the EM calorimeter, the size of the hadronic calorimeter, the efficiencies of momentum reconstruction in the tracker and the efficiencies of energy deposition to the calorimeters. The Muon Collider Community has designed such a `Delphes` card for the Muon Collider Detector (see reference [38]), which was used for the research in this thesis. As explained in reference [38]: The parameterisation of the Muon Collider (Detector) is intended as a target performance; a hybrid between the performance of the FCC-hh[20] and the CLIC[21], and has not been validated by full simulation.

3.2 Validation

Let us start with an analysis of the simulation without EW Bremsstrahlung. This section compares theoretical predictions with results from the simulation and therefore serves as a validation of the simulation.

Kinematics Higgs and Z boson The kinematics of the Higgs and the Z boson can be predicted theoretically. Since the total initial momentum is zero, we expect the Higgs boson to have a momentum of equal magnitude as the Z boson, but in exactly the opposite direction. Figure 11 shows that the magnitude of the momentum is indeed the same for the Higgs and the Z boson. Furthermore, considering the x, y, and z-components of the momenta individually, we see that each

[17] These software packages are available online. `MadGraph 5` was taken from `http://madgraph.phys.ucl.ac.be/`; the version used is 2.8.0. The `Pythia 8` version used, has recently been released as version series `Pythia 8.3` at `https://pythia.org/releases/`. `Delphes` version 3.4.2 was taken from `https://cp3.irmp.ucl.ac.be/projects/delphes`.

[18] When EW Bremsstrahlung is switched on, dipole QED + weak showers are simulated. [35]

[19] When EW Bremsstrahlung is turned off, only dipole QED showers are simulated. [35]

[20] FCC-hh is short for Future Circular Collider that collides hadrons.

[21] CLIC is short for Compact LInear Collider, intended to collide electrons and positrons.

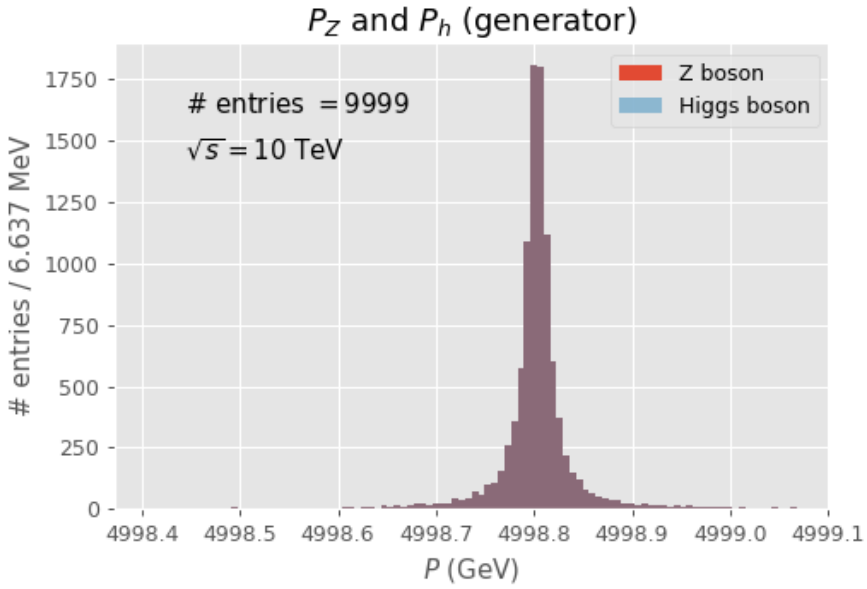

Figure 11: *Histogram of the magnitudes of momenta of the Higgs and Z boson at generator level. As expected, these are equal, such that the two histograms exactly overlap one another.*

momentum component of the Higgs boson exactly cancels the same component of the Z boson. This is shown in table 1 for the first ten events.

Event	P_x h **(GeV)**	P_x Z **(GeV)**	P_y h **(GeV)**	P_y Z **(GeV)**	P_z h **(GeV)**	P_z Z **(GeV)**
0	520.8704	-520.8704	-4735.8213	4735.8213	-1512.8209	1512.8209
1	1121.0879	-1121.0879	-1175.6774	1175.6774	-4727.454	4727.454
2	4688.3833	-4688.3833	1669.2417	-1669.2417	-471.2065	471.2065
3	-2624.9329	2624.9329	-2851.084	2851.084	3157.362	-3157.362
4	-3932.4397	3932.4397	-2400.0625	2400.0625	1940.1254	-1940.1254
5	-4566.6733	4566.6733	775.133	-775.133	1879.5117	-1879.5117
6	-942.78	942.78	-4033.4678	4033.4678	2798.2473	-2798.2473
7	-2826.7769	2826.7769	3545.6948	-3545.6948	-2103.6672	2103.6672
8	203.01694	-203.01694	-4443.7705	4443.7705	-2280.2883	2280.2883
9	1029.3372	-1029.3372	-3857.6257	3857.6257	-3007.8337	3007.8337

Table 1: *The components of the momenta of the Higgs and Z boson for the first ten events of the simulation without EW Bremsstrahlung at $\sqrt{s} = 10$ TeV. h and Z represent the Higgs and the Z boson respectively. Each momentum component of the Higgs boson exactly cancels the same component of the Z boson.*

The total CM energy of 10 TeV should be conserved, so the energies of the Higgs and the Z boson must add up to 10 TeV. Figure 12 shows that this is indeed the case.

Let us calculate what the exact energies and momenta of the bosons should be. We know

$$\sqrt{s} = E_Z + E_h \tag{7}$$

$$\boldsymbol{p}_Z = -\boldsymbol{p}_h \tag{8}$$

Using the definition $p \equiv |\boldsymbol{p}_Z| = |\boldsymbol{p}_h|$ together with $E = \sqrt{p^2 + m^2}$, we can write equation (7) as

$$\sqrt{s} = \sqrt{m_Z^2 + p^2} + \sqrt{m_h^2 + p^2}$$

Reordering and squaring yields:

$$m_h^2 + p^2 = s + m_Z^2 + p^2 - 2\sqrt{s}\sqrt{m_Z^2 + p^2}$$

p^2 cancels and the rest be rearranged to:

$$2\sqrt{s}\sqrt{m_Z^2 + p^2} = s + m_Z^2 - m_h^2$$

Squaring and solving for p, we find:

$$p = \frac{\sqrt{\lambda\left(s, m_Z^2, m_h^2\right)}}{2\sqrt{s}} \tag{9}$$

with $\lambda\left(s, m_Z^2, m_h^2\right) = s^2 + m_Z^4 + m_h^4 - 2sm_Z^2 - 2sm_h^2 - 2m_Z^2 m_h^2$; the Källén function. We now have the exact magnitude of momentum of the two bosons. Let us also find the energies of the bosons. To this end, we substitute equation (9) into $E_Z = \sqrt{m_Z^2 + p^2}$:

$$\begin{aligned}
E_Z &= \sqrt{m_Z^2 + \frac{1}{4}\left(s + \frac{m_Z^4 + m_h^4 - 2m_Z^2 m_h^2}{s} - 2\left(m_Z^2 + m_h^2\right)\right)} \\
&= \frac{1}{2}\sqrt{s + \frac{\left(m_Z^2 - m_h^2\right)^2}{s} + 2\left(m_Z^2 - m_h^2\right)} \\
&= \frac{1}{2\sqrt{s}}\sqrt{s^2 + 2s\left(m_Z^2 - m_h^2\right) + \left(m_Z^2 - m_h^2\right)^2} \\
&= \frac{1}{2\sqrt{s}}\sqrt{\left(s + m_Z^2 - m_h^2\right)^2} \\
&= \frac{s + m_Z^2 - m_h^2}{2\sqrt{s}}
\end{aligned}$$

Along the same lines, by substituting $Z \to h$ and $h \to Z$, we find the energy of the Higgs boson. Ultimately, we obtain the following relations for the magnitude of momentum and the energies of the Z and Higgs bosons:

$$p_{Z,h} = \frac{\sqrt{\lambda\left(s, m_Z^2, m_h^2\right)}}{2\sqrt{s}} \tag{10}$$

$$E_Z = \frac{s + m_Z^2 - m_h^2}{2\sqrt{s}} \tag{11}$$

$$E_h = \frac{s + m_h^2 - m_Z^2}{2\sqrt{s}} \tag{12}$$

Evaluating these three equations using[22] $\sqrt{s} = 10$ TeV, $m_Z = 91.188$ GeV and $m_h = 125.000$ GeV, we obtain the results shown in table 2. The results from the simulation are in accordance with the theoretical predictions; see also figures 11 and 12. The small differences between the theoretical prediction and the result of the simulation can be attributed to the fact that the masses in the simulation are resonances rather than fixed masses; they are distributed according to the Breit-Wigner distribution. Simulating more events would reduce the differences between the predictions and the simulation.

Jet kinematics The $h \to b\bar{b}$ decay results in the formation of two jets. By plotting the locations and momenta of the final-state particles per event, we can easily distinguish the jets as a tight bunch of particles (see figure 13). For each event we also see the two neutrinos, which have a difference of approximately π radians to the jets in the ϕ direction. In the η direction, the neutrinos have

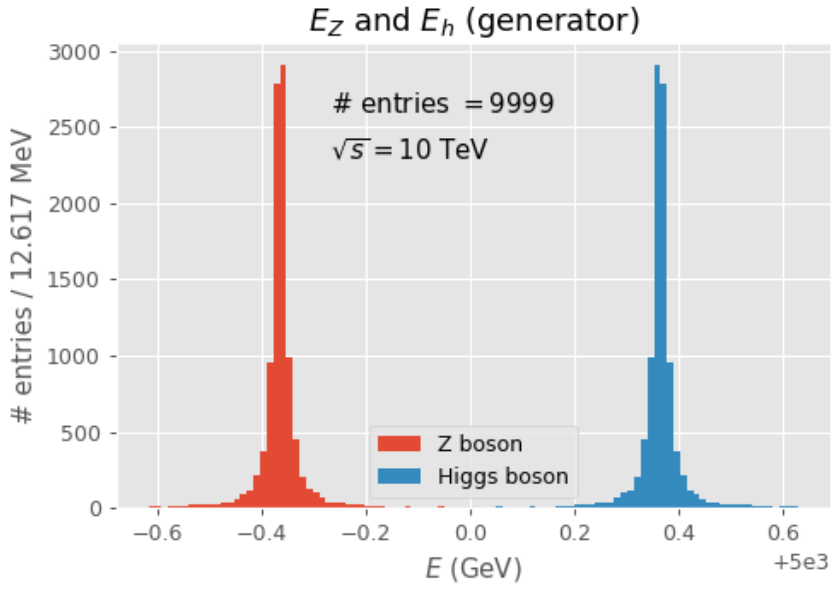

Figure 12: *Histogram of the energies of the Higgs and Z boson at generator level.*

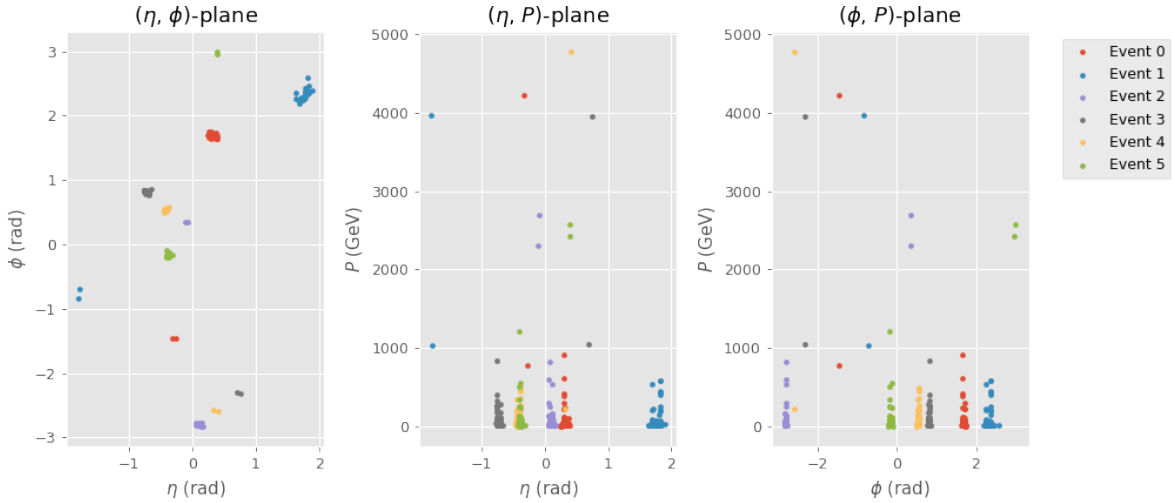

Figure 13: *Kinematics of the final-state particles in the generator. The first plot shows azimuthal angle ϕ against pseudorapidity η. For each event, we clearly see one group of particles representing the two jets. We also see for each event two neutrinos, having an azimuthal distance of π radians from the jets and having the same $|\eta|$ as the jets. Consequently, we can conclude that the neutrinos move opposite from the jets. The second and third plots show the total momentum P (in GeV) versus pseudorapidity η and azimuthal angle ϕ respectively.*

	Prediction (GeV)	**Simulation (GeV)**
$p_{Z,h}$	4998.80	4998.80 ± 0.05
E_Z	4999.63	4999.64 ± 0.05
E_h	5000.37	5000.36 ± 0.05

Table 2: *The theoretical predictions and the results from the simulations for the kinematics of the Z and Higgs bosons. The results from the simulation follow from averaging over all 9999 events with one standard deviation as the uncertainty.*

approximately the same $|\eta|$ as the jets. Thus, we can conclude that the neutrinos indeed oppose the jets.

We expect two jets per event, but rather see just one. However, on closer inspection, the jets simply lie too close to each other to distinguish them easily: Zooming in allows us to tell them apart (although not for all events). To demonstrate, figure 14 shows P (in GeV) against η zoomed in on six different events. Indeed, most events show a clear separation between the jets.

Jet multiplicity As explained in section 2.4, the jets are reconstructed using the jet reconstruction algorithm Valencia. From the $h \to b\bar{b}$ decay, we expect two jets: one from the b-quark and one from the $\bar{b}$-quark. However, when using inclusive clustering with the smallest R possible[23] ($R = 0.2$), almost all events show only a single reconstructed jet! At the detector level, six out of 9999 events have no reconstructed jets, 9817 events have only a single reconstructed jet and 176 events have two reconstructed jets.

The fact that, in most events, the reconstruction algorithm finds only one jet may be due to the high CM energy of 10 TeV. After all, it gives the Higgs boson a momentum of approximately 5 TeV, which makes it undergo a high Lorentz boost. Due to this boost, the two jets into which the Higgs boson decays become highly collimated; see Appendix B for more details.

It is possible that the jets are too close to one another for the reconstruction algorithm to resolve both jets. In fact, when simulating the same physics at a lower CM energy of 400 GeV, much more events have two reconstructed jets: 5150 out of 9999 at detector level.

3.3 Reconstructing the Higgs boson

Using the two jets which follow from the $h \to b\bar{b}$ decay, the Higgs mass can be reconstructed. As shown in section 3.2, the inclusive jet reconstruction algorithm cannot resolve both jets in most events. However, exploiting the *exclusive* reconstruction algorithm, a two-jet output can be forced. In the end, Valencia[24] yields the transverse momentum p_T, pseudorapidity η, azimuthal angle ϕ and mass m for each jet. These quantities can be used to find the combined invariant mass of the jets, as follows:

First, the three-momenta are calculated using the relations below:

$$\begin{aligned} p_x &= p_T \cos\phi \\ p_y &= p_T \sin\phi \\ p_z &= p_T \sinh\eta \end{aligned}$$

Next, the energies of the jets are calculated using:

$$E_i = \boldsymbol{p}_i \cdot \boldsymbol{p}_i + m_i^2 \quad \text{with} \quad i \in \{1, 2\}$$

where 1 and 2 represent jet 1 and jet 2 respectively and the boldface symbols are used for three-vectors. The combined invariant mass is then calculated from:

$$m_{inv} = E_1 + E_2 - (\boldsymbol{p}_1 + \boldsymbol{p}_2) \cdot (\boldsymbol{p}_1 + \boldsymbol{p}_2) \tag{13}$$

Using equation (13) together with the lowest jet-radius value possible[25], $R = 0.5$, we can recon-

[22] `MadGraph 5` uses $m_h = 125.000$ GeV and $m_Z = 91.188$ GeV. Hence, these are the values used in this calculation.

[23] As explained in section 2.4, R is a measure for the maximum allowed size of a jet. The smaller R, the smaller the jet is allowed to be.

[24] Valencia is the jet reconstruction algorithm used throughout this thesis, see section 2.4.

[25] Note that 0.5 is the lowest possible R for *exclusive* clustering; for inclusive clustering the minimum is 0.2.

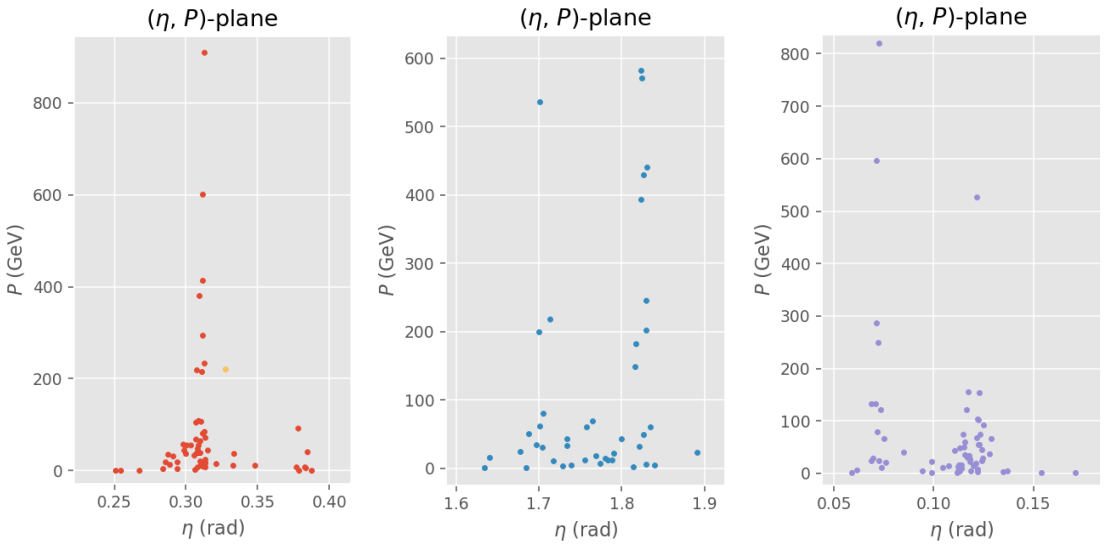

(a) *Event 0*

(b) *Event 1*

(c) *Event 2*

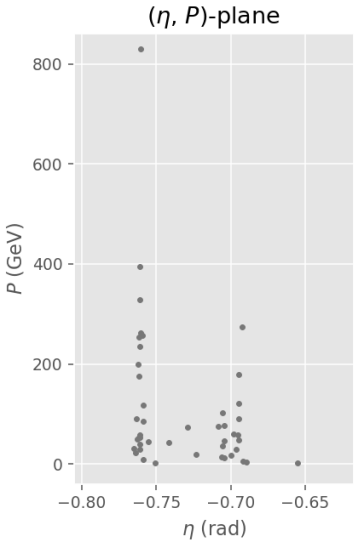

(d) *Event 3*

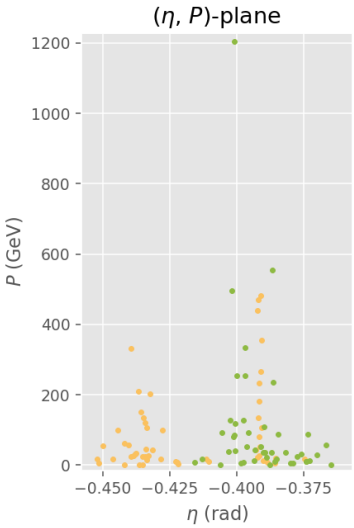

(e) *Events 4 and 5*

Figure 14: *Total momentum P (in GeV) versus pseudorapidity η zoomed in on different events. In most events, we can resolve the two jets by zooming in sufficiently far.*

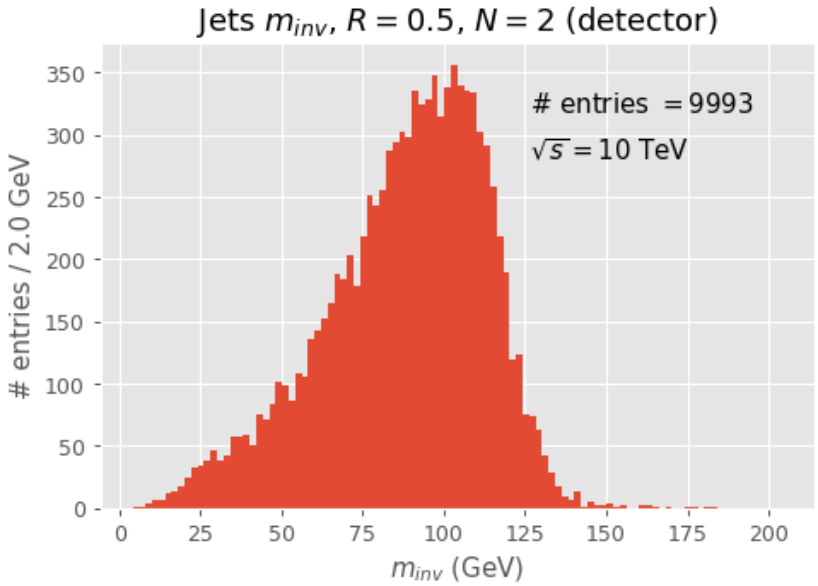

Figure 15: *Histogram of the invariant mass of the two jets into which the Higgs boson decays. The jets were reconstructed using an exclusive jet clustering algorithm set to* $R = 0.5$.

struct the Higgs mass reasonably well from the two jets (see figure 15). It is striking that the mass distribution peaks around 100 GeV, whereas the actual Higgs mass peaks at 125 GeV. Possible causes for this include:

1. The jets radiate photons and gluons (i.e. Bremsstrahlung[26]) that are not accounted for in the exclusive jet reconstruction. By forcing the algorithm to find two jets, it could be that only the two collimated b-jets are reconstructed and that the jet(s) formed by gluon Bremsstrahlung is (are) not reconstructed at all.

2. The jet reconstruction algorithm has an insufficiently large R and thereby excludes particles that actually belong to the jets.

3. Not all particles are detected, due to low detector resolution.

The following thought experiment shows that the reasons above may indeed cause the reconstructed mass to be lower: Imagine the Higgs boson in its rest frame. The boson then decays into a b- and an $\bar{b}$-quark, leading to different types of hadrons that move in all directions and belong to two jets. The total momentum must add up to zero (since we are in the rest frame of the Higgs) and the total energy must equal the mass of the Higgs boson. Now suppose that some hadrons are taken out of the system (i.e. they are not used in the reconstruction or not all particles are detected). We are left with less energy and with nonzero total momentum. Therefore, $m^2 = E^2 - p^2$ will always be smaller than the original invariant mass m_h. As a result, the reconstructed mass is lower than the actual Higgs mass. In the following three paragraphs, the possible causes mentioned above are investigated.

Bremsstrahlung of photons and gluons Figure 16 shows the locations of final-state particles at generator level and reconstructed jets at detector level, in four individual events where some particles are 'far'[27] from the the jets. From this figure, we can tell that there are indeed events where Bremsstrahlung of photons (and possibly gluons) occurs. It is interesting to see in how many events this occurs and what particles are located far away from the jets. This is shown in figure

[26] Note that this does not include EW Bremsstrahlung. EW bosons are not radiated, but rather only photons and gluons.

[27] 'Far' is defined as $\sqrt{(\Delta\eta)^2 + (\Delta\phi)^2} > 0.2$, so that it captures particles that are most likely not used in the jet reconstruction.

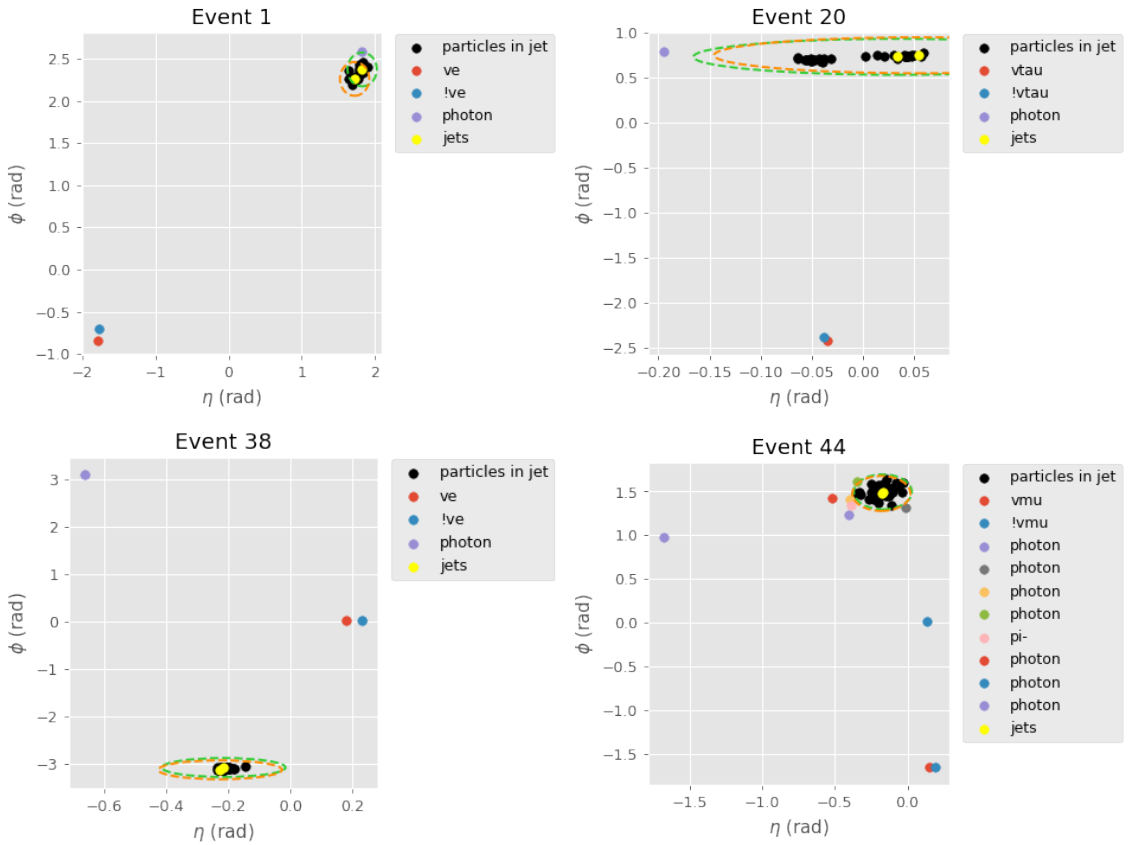

Figure 16: *Locations of final-state particles and reconstructed jets in (η, ϕ)-space for four events. The yellow dots represent the reconstructed jets at detector level. All other dots are final-state particles at generator level. The two dashed ellipses are boundaries indicating whether or not particles are 'far' from the reconstructed jets. Particles inside one of the ellipses are coloured black. Particles outside both ellipses have their own colour. The legend shows the types of particles outside the dashed lines. An exclamation mark in front of a symbol indicates a neutral antiparticle.*

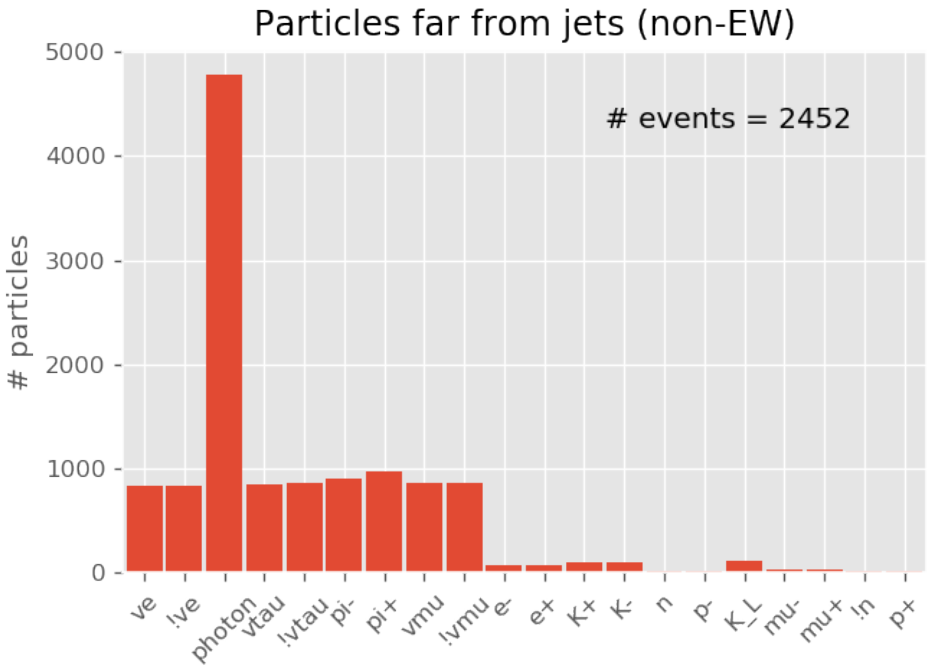

Figure 17: *Histogram of final-state particles at generator level that are 'far' from the reconstructed jets at detector level. For charged particles, the sign behind the symbol indicates whether it is a particle or antiparticle. For neutral particles, an exclamation mark in front of the symbol indicates an antiparticle.*

17. 2452 out of 9999 events have particles that are located far from the reconstructed jets (apart from the two neutrinos originating from the Z boson) that can be attributed to Bremsstrahlung. Photons are by far most frequently located far from the jets: On average (over all 9999 events) there are approximately 0.5 photons far from the jets per event, compared to, on average, approximately 0.1 pions (π^+ or π^-). Other stray particles are negligible.

Since only 2452 out of 9999 events have 'Bremsstrahlung-behaviour', the Bremsstrahlung of photons or gluons cannot be the main cause for the low reconstructed Higgs mass. However, it definitely contributes.

Insufficiently large R The $R = 0.5$ used in the jet reconstruction could be too small, meaning that jet constituents are excluded from the jets during reconstruction. If this were the case, a larger R would result in a mass reconstruction closer to the real Higgs mass. However, figure 18 shows that there is no significant difference between using the smallest R ($R = 0.5$) and the largest R ($R = 1.5$). Hence, it is unlikely that the reconstructed combined jet mass is too low due to insufficiently large R in the jet reconstruction. It might, however, be that even $R = 1.5$ is too small, and that larger values need to be considered. Such values for R are not implemented in the `Delphes` simulation, so this is not further investigated in this thesis.

Not all particles detected The low reconstructed Higgs mass may also be due to not all particles being detected. `Delphes` acquires information about the tracker and the EM and hadronic calorimeters, and combines this information to reconstruct particle-flows [37]. Three different particle-flow branches are created: particle-flow tracks for charged particles, particle-flow towers for photons and particle-flow towers for neutral hadrons. Combined, these branches should give information about all detected particles. Comparing this information from the detector with the information on generator level, we can find out whether or not all particles are detected.

Figure 19 shows the percentage of particles that are present at generator level, but are not present in the particle-flow data sets. Roughly 20% of the particles are not included in the particle-flow algorithm. It is interesting to see how this 20% is distributed over the different detector parts.

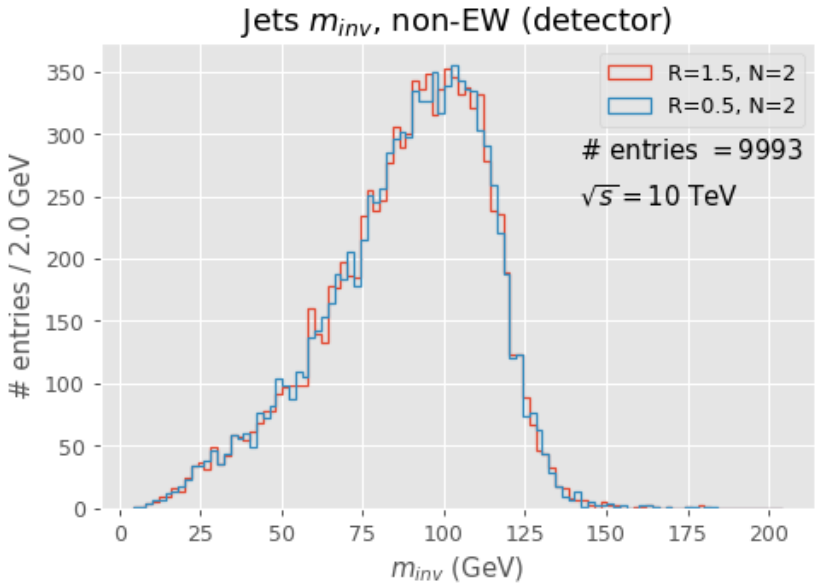

Figure 18: *Histograms of the invariant mass of the two jets into which the Higgs boson decays, for* $R = 0.5$ *(blue) and* $R = 1.5$ *(red) where* R *is the jet-size parameter used in the jet reconstruction algorithm.*

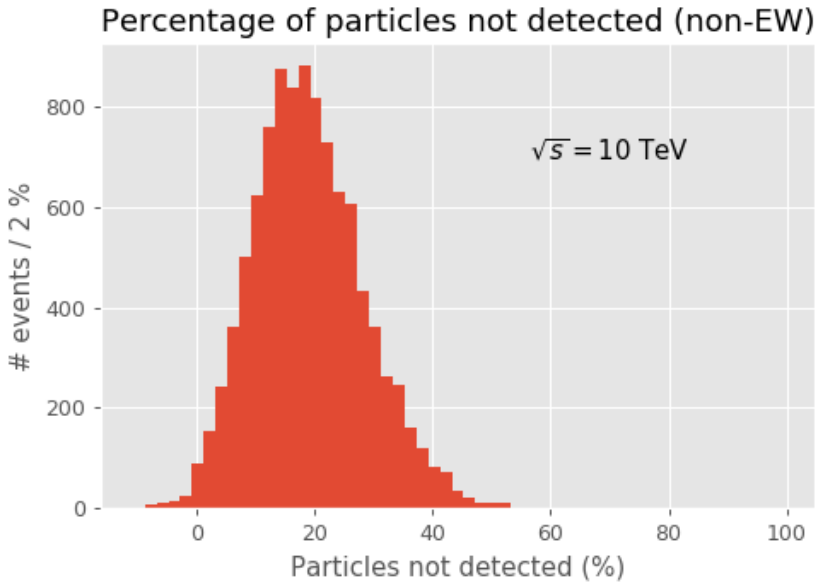

Figure 19: *Histogram of percentages of the particles that are not present in the particle-flow data sets (neutrinos excluded). Negative percentages mean that some particles are present in the particle-flow data sets, but are not present at generator level.*

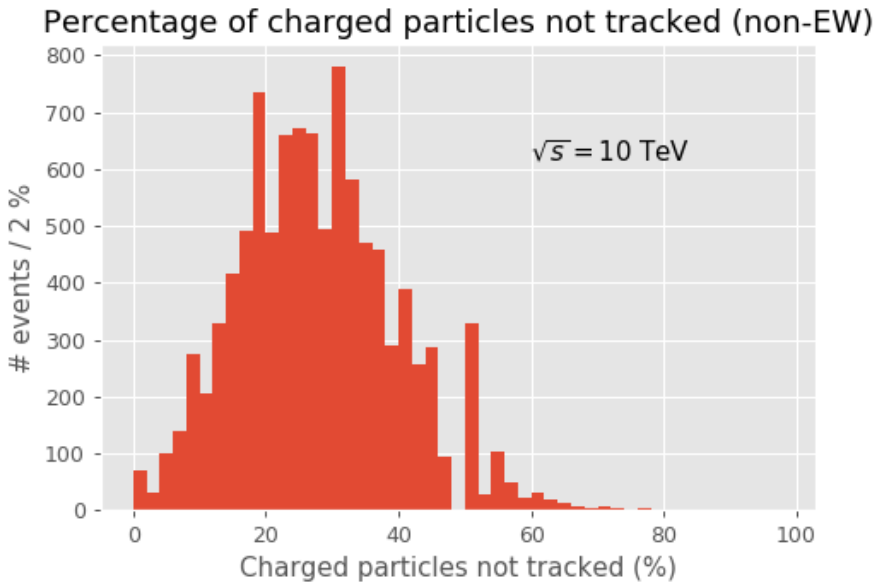

Figure 20: *Histogram of percentages of charged particles that are not present in the particle-flow 'Track' data set. Negative percentages mean that some particles are present in the particle-flow data set, but are not present at generator level.*

Figures 20, 21 and 22 show the percentages of respectively charged particles, photons and neutral hadrons that are present at generator level, but are not present in the corresponding particle-flow data set. Negative percentages mean that particles are present in the particle-flow data set, but not at generator level, i.e. they are 'fake' or unjustly identified particles. Apparently, on average, for about 25% of charged particles and photons are not included in the particle-flow algorithm. Hence, it is not just the tracker or just a calorimeter that does not operate well. It is also remarkable that many neutral hadrons are 'observed' that are not actually there.

The fact that 25% of the charged particles and photons are not present in the particle-flow, may be due to these particles being detected neither by the tracker, the EM calorimeter nor the hadronic calorimeter. Another possibility is that the particle-flow algorithm is incomplete, failing to take all particles into account. If the former is the case, it is a very likely cause for the low reconstructed Higgs mass. If the latter is the case, the cause of the low reconstructed mass remains unclear.

3.4 Reconstructing the Z boson

In the simulation $Z \to \nu\overline{\nu}$ and, as explained in section 2.2, neutrinos typically escape the detector and are therefore not measured. Consequently, some energy and momentum is missing. From this deficit, we can determine the missing invariant mass. If the two neutrinos are the only particles not detected, this missing mass should match the mass of the Z boson. Let us have a look whether or not this is the case.

First, the missing mass is calculated from the same two jets used in the reconstruction of the Higgs mass (section 3.3). The following relations are used:

$$E_{\text{miss}} = \sqrt{s} - E_{\text{jet1}} - E_{\text{jet2}} \tag{14}$$

$$\boldsymbol{p}_{\text{miss}} = -\left(\boldsymbol{p}_{\text{jet1}} + \boldsymbol{p}_{\text{jet2}}\right) \tag{15}$$

Then, the missing mass is found by:

$$m_{\text{miss}} = \sqrt{E_{\text{miss}}^2 - \boldsymbol{p}_{\text{miss}}^2} \tag{16}$$

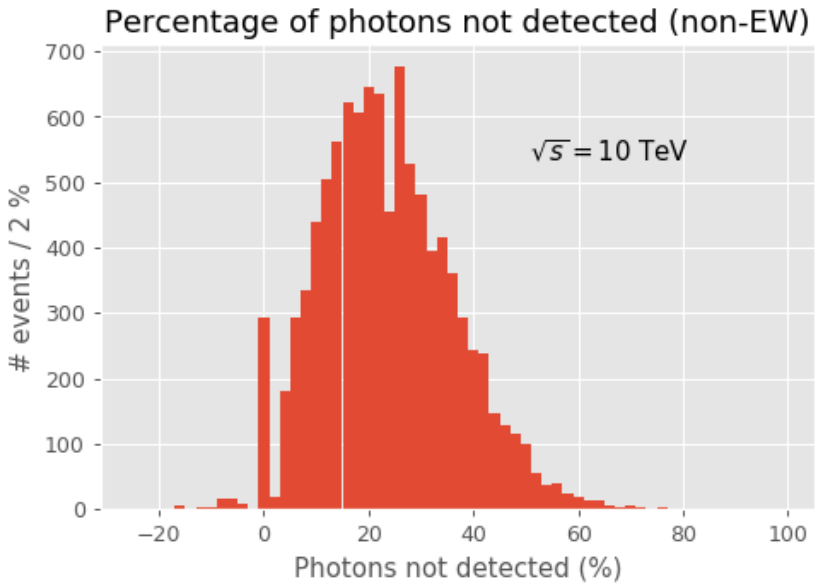

Figure 21: *Histogram of percentages of photons that are not present in the particle-flow 'Photon' data set. Negative percentages mean that some particles are present in the particle-flow data set, but are not present at generator level.*

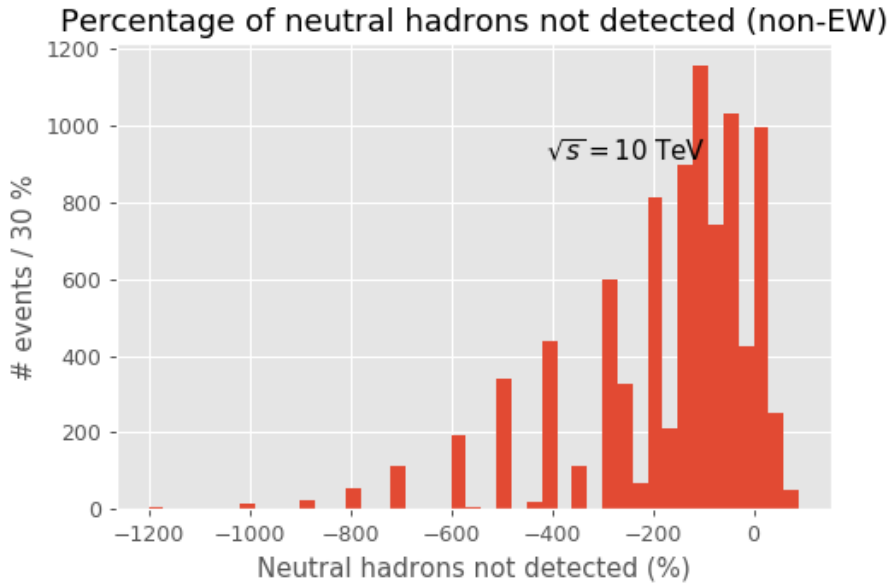

Figure 22: *Histogram of percentages of neutral hadrons that are not present in the particle-flow 'NeutralHadron' data set. Negative percentages mean that some particles are present in the particle-flow data set, but are not present at generator level.*

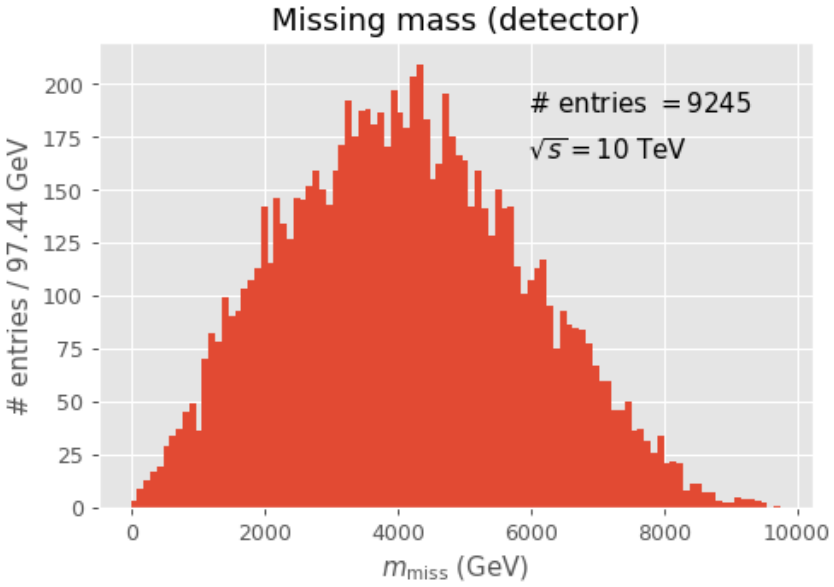

Figure 23: *Histogram of the missing invariant mass, calculated from the same jets used in the Higgs reconstruction;* $\sqrt{s} = 10$ *TeV.*

These calculations lead to the missing mass distribution in figure 23. This clearly does not resemble the mass distribution of the Z boson, which should peak around 91 GeV.[28]

Let us try another method to calculate the missing mass: particle-flows. As explained in section 3.3, `Delphes` creates three particle-flow branches containing information about the tracker and the EM and hadronic calorimeters. The particle-flow tracks yield momentum P, transverse momentum P_T, pseudorapidity η and azimuthal angle ϕ. The particle-flow towers return energy E, transverse energy E_T, pseudorapidity η and azimuthal angle ϕ. These values are used to find the three-momenta. For tracks:

$$\begin{aligned} P_x &= P_T \cos\phi \\ P_y &= P_T \sin\phi \\ P_z &= P_T \sinh\eta \end{aligned}$$

And for towers:

$$\begin{aligned} P_x &= E_T \cos\phi \\ P_y &= E_T \sin\phi \\ P_z &= E_T \sinh\eta \end{aligned}$$

Then, for each event, the total energy E_{tot} and total three-momentum $\boldsymbol{P}_{\text{tot}}$ is determined, by summing the appropriate components of the elements in the particle-flow tracks and towers. These are then used to find the missing energy and momentum, $E_{\text{miss}} = \sqrt{s} - E_{\text{tot}}$ and $\boldsymbol{P}_{\text{miss}} = -\boldsymbol{P}_{\text{tot}}$, which in turn lead to the missing invariant mass $m_{\text{miss}} = \sqrt{E_{\text{miss}}^2 - \boldsymbol{P}_{\text{miss}} \cdot \boldsymbol{P}_{\text{miss}}}$.

Applying this calculation to the data from the simulation, the mass distribution in figure 24 is obtained[29].

This also does not match the mass distribution of the Z boson. Possible causes are:

1. Much energy escapes the detector through the beam openings, therefore the missing energy is high. Momentum also escapes through the beam openings, yet due to the nature of

[28] Since the reconstructed Higgs mass was too low, the peak of the reconstructed missing mass is not expected exactly at 91 GeV. However, a peak at 4000 GeV is very high.

[29] Some events have $E_{\text{tot}}^2 < \boldsymbol{P}_{\text{miss}} \cdot \boldsymbol{P}_{\text{miss}}$, being nonphysical and resulting in a negative value in the square root. This is probably due to the resolutions of the tracker and the calorimeters. These events are left out. Hence, there are only 9153 plotted.

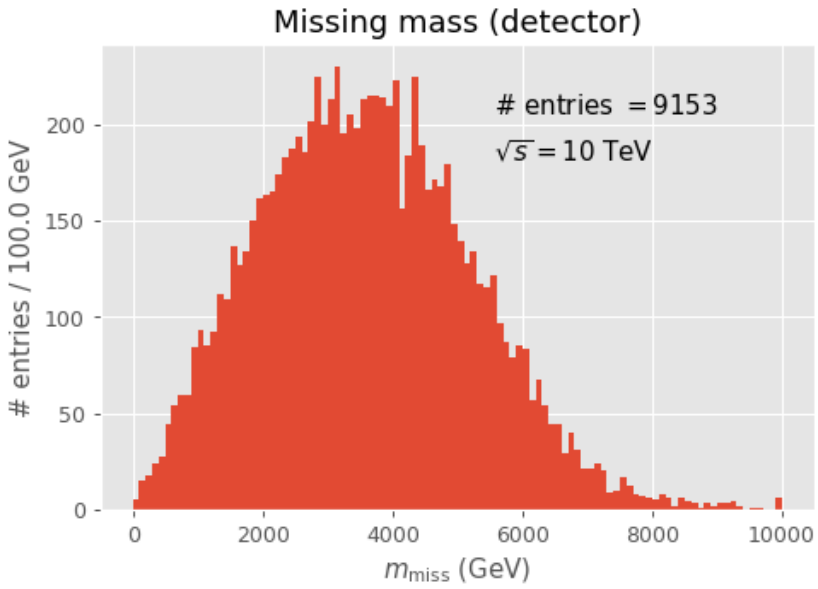

Figure 24: *Histogram of the missing invariant mass, calculated using particle-flows from* `Delphes` *at* $\sqrt{s} = 10$ *TeV.*

momentum (i.e. being a vector quantity) escaping momenta on opposite sides of the detector approximately cancel. Since energy is a scalar, the energies escaping on both sides of the detector do not cancel, but rather add up. Consequently, $m^2_{\text{miss,measured}} = E^2_{\text{miss,measured}} - \boldsymbol{P}^2_{\text{miss,measured}} > E^2_{\text{miss,truth}} - \boldsymbol{P}^2_{\text{miss,truth}} = m^2_{\text{miss,truth}}$ and we reconstruct a missing invariant mass that is certainly too large.

2. The detector has insufficient resolution, causing the uncertainty in measuring E_{tot} and $\boldsymbol{P}_{\text{tot}}$ to be large, resulting in the uncertainty on m_{miss} being so large that we cannot resolve any peaks around the Z mass.

3. Apart from the two neutrinos belonging to the Z boson, it could be that not all particles (from the two jets of the Higgs boson) are detected or taken into account in the calculation[30]. These particles contribute to missing energy. However, since their momentum is in the direction of the jets, they contribute negatively to the missing momentum, meaning part of the Higgs momentum is not measured. Consequently the missing momentum (i.e. opposite of Higgs momentum) works out to be too low. In conjunction with an excess of missing energy, this results in an enlarged missing invariant mass.

Let us investigate which of these three could cause the strange missing mass distribution.

Particles escaping through beams The detector has openings through which the muon beams enter. Through these same openings, particles may also escape the detector, resulting in an overestimation of the missing mass. In the `Delphes` Card of the Muon Collider Detector [38], both the EM calorimeter and the hadronic calorimeter reach a maximum pseudorapidity $\eta = 2.5$, which corresponds to a minimum angle $\theta = 2 \arctan\left[\exp\left(-2.5\right)\right] \approx 9.4°$. So, whenever a particle at generator level is located at an angle $\theta < 9.4°$ or $\theta > 180° - 9.4° = 170.6°$, it will escape the detector through the beam opening. Looking at the data from the simulation, it appears that only 32 out of 9999 events feature particles with $\theta < 9.4°$ or $\theta > 170.6°$. Hence, particles escaping through the beam openings cannot be a valid cause for the large missing mass distribution.

Detector resolution If the detector resolution is low, E_{tot} and $\boldsymbol{P}_{\text{tot}}$ are measured with a large uncertainty, resulting in a very broad distribution of missing mass. We can characterise the width

[30] E.g. neutrinos created in the jets or muons that may not be reconstructed in the particle-flows.

of this distribution by the standard deviation σ. If σ is too large, the peak around the Z mass cannot be resolved. Let us determine the minimum resolution for measuring E_{tot} and $\boldsymbol{P}_{\text{tot}}$, so that the Z peak can still be resolved.

Defining $P_{\text{tot}} \equiv |\boldsymbol{P}_{\text{tot}}|$, the missing mass m_{miss} is calculated according to:

$$m_{\text{miss}} = \sqrt{E_{\text{miss}}^2 - P_{\text{tot}}^2} = \sqrt{\left(\sqrt{s} - E_{\text{tot}}\right)^2 - P_{\text{tot}}^2} = \sqrt{s - 2\sqrt{s}E_{\text{tot}} + E_{\text{tot}}^2 - P_{\text{tot}}^2} \tag{17}$$

We can determine the uncertainty (or standard deviation) on m_{miss} by applying propagation of uncertainty:

$$\sigma_{m_{\text{miss}}}^2 = \left(\frac{\partial m_{\text{miss}}}{\partial E_{\text{tot}}}\right)^2 \sigma_{E_{\text{tot}}}^2 + \left(\frac{\partial m_{\text{miss}}}{\partial P_{\text{tot}}}\right)^2 \sigma_{P_{\text{tot}}}^2 + 2\left(\frac{\partial m_{\text{miss}}}{\partial E_{\text{tot}}}\right)\left(\frac{\partial m_{\text{miss}}}{\partial P_{\text{tot}}}\right)\sigma_{E_{\text{tot}},P_{\text{tot}}} \tag{18}$$

with covariance $\sigma_{E_{\text{tot}},P_{\text{tot}}} = \sigma_{E_{\text{tot}}}\sigma_{P_{\text{tot}}}\rho_{E_{\text{tot}},P_{\text{tot}}}$ where $\rho_{E_{\text{tot}},P_{\text{tot}}}$ is the correlation coefficient:

$$\rho_{E_{\text{tot}},P_{\text{tot}}} = \begin{cases} 1 & \text{if 100\% correlated} \\ -1 & \text{if 100\% anti-correlated} \end{cases} \tag{19}$$

E_{tot} and P_{tot} are definitely correlated: If P_{tot} is large, E_{tot} must be large as well. Although we do not know what their exact correlation coefficient is, we do know it must be somewhere between 0 and 1. Calculating the required resolution using both of these correlation coefficients, we can set an upper bound for the uncertainty on E_{tot} and P_{tot}, i.e. the smallest $\sigma_{E_{\text{tot}}}$ and $\sigma_{P_{\text{tot}}}$ of the two cases. Suppose $\rho_{E_{\text{tot}},P_{\text{tot}}} = 1$, then equation (18) becomes:

$$\sigma_{m_{\text{miss}}}^2 = \left(\frac{-2\sqrt{s} + 2E_{\text{tot}}}{2m_{\text{miss}}}\right)^2 \sigma_{E_{\text{tot}}}^2 + \left(\frac{-2P_{\text{tot}}}{2m_{\text{miss}}}\right)^2 \sigma_{P_{\text{tot}}}^2 + 2\left(\frac{-2\sqrt{s} + 2E_{\text{tot}}}{2m_{\text{miss}}}\right)\left(\frac{-2P_{\text{tot}}}{2m_{\text{miss}}}\right)\sigma_{E_{\text{tot}}}\sigma_{P_{\text{tot}}}$$

$$\sigma_{m_{\text{miss}}}^2 = \left(\frac{s - 2\sqrt{s}E_{\text{tot}} + E_{\text{tot}}^2}{m_{\text{miss}}^2}\right)\sigma_{E_{\text{tot}}}^2 + \left(\frac{P_{\text{tot}}^2}{m_{\text{miss}}^2}\right)\sigma_{P_{\text{tot}}}^2 + 2\left(\frac{P_{\text{tot}}\sqrt{s} - P_{\text{tot}}E_{\text{tot}}}{m_{\text{miss}}^2}\right)\sigma_{E_{\text{tot}}}\sigma_{P_{\text{tot}}} \tag{20}$$

Looking at equation (17), we can rewrite the numerator in the first term:

$$\sigma_{m_{\text{miss}}}^2 = \left(\frac{m_{\text{miss}}^2 + P_{\text{tot}}^2}{m_{\text{miss}}^2}\right)\sigma_{E_{\text{tot}}}^2 + \left(\frac{P_{\text{tot}}^2}{m_{\text{miss}}^2}\right)\sigma_{P_{\text{tot}}}^2 + \left(\frac{2P_{\text{tot}}\sqrt{s} - 2P_{\text{tot}}E_{\text{tot}}}{m_{\text{miss}}^2}\right)\sigma_{E_{\text{tot}}}\sigma_{P_{\text{tot}}}$$

$$\sigma_{m_{\text{miss}}}^2 = \left(1 + \frac{P_{\text{tot}}^2}{m_{\text{miss}}^2}\right)\sigma_{E_{\text{tot}}}^2 + \left(\frac{P_{\text{tot}}^2}{m_{\text{miss}}^2}\right)\sigma_{P_{\text{tot}}}^2 + \left(\frac{2P_{\text{tot}}\sqrt{s} - 2P_{\text{tot}}E_{\text{tot}}}{m_{\text{miss}}^2}\right)\sigma_{E_{\text{tot}}}\sigma_{P_{\text{tot}}}$$

$$\sigma_{m_{\text{miss}}}^2 = \sigma_{E_{\text{tot}}}^2 + \left(\frac{P_{\text{tot}}^2}{m_{\text{miss}}^2}\right)\left(\sigma_{E_{\text{tot}}}^2 + \sigma_{P_{\text{tot}}}^2\right) + \left(\frac{2P_{\text{tot}}\sqrt{s} - 2P_{\text{tot}}E_{\text{tot}}}{m_{\text{miss}}^2}\right)\sigma_{E_{\text{tot}}}\sigma_{P_{\text{tot}}} \tag{21}$$

Again using equation (17), we can write:

$$m_{\text{miss}}^2 = s - 2\sqrt{s}E_{\text{tot}} + E_{\text{tot}}^2 - P_{\text{tot}}^2$$

Reordering gives:

$$E_{\text{tot}}^2 - 2\sqrt{s}E_{\text{tot}} + s - P_{\text{tot}}^2 - m_{\text{miss}}^2 = 0$$

The quadratic formula then gives:

$$E_{\pm} = \frac{2\sqrt{s} \pm \sqrt{4s - 4s + 4P_{\text{tot}}^2 + 4m_{\text{miss}}^2}}{2}$$

$$E_{\pm} = \sqrt{s} \pm \sqrt{P_{\text{tot}}^2 + m_{\text{miss}}^2} \tag{22}$$

$E_{\text{tot}} > \sqrt{s}$ would be nonphysical; the only physically allowed solution is E_-. Substituting equation (22) into equation (21) yields:

$$\sigma^2_{m_{\text{miss}}} = \sigma^2_{E_{\text{tot}}} + \left(\frac{P^2_{\text{tot}}}{m^2_{\text{miss}}}\right)\left(\sigma^2_{E_{\text{tot}}} + \sigma^2_{P_{\text{tot}}}\right) + \left(\frac{2P_{\text{tot}}\sqrt{s} - 2P_{\text{tot}}\sqrt{s} + 2P_{\text{tot}}\sqrt{P^2_{\text{tot}} + m^2_{\text{miss}}}}{m^2_{\text{miss}}}\right)\sigma_{E_{\text{tot}}}\sigma_{P_{\text{tot}}}$$

$$\sigma^2_{m_{\text{miss}}} = \sigma^2_{E_{\text{tot}}} + \left(\frac{P^2_{\text{tot}}}{m^2_{\text{miss}}}\right)\left(\sigma^2_{E_{\text{tot}}} + \sigma^2_{P_{\text{tot}}}\right) + \left(\frac{2P_{\text{tot}}\sqrt{P^2_{\text{tot}} + m^2_{\text{miss}}}}{m^2_{\text{miss}}}\right)\sigma_{E_{\text{tot}}}\sigma_{P_{\text{tot}}} \tag{23}$$

Now, suppose $\sigma_{E_{\text{tot}}} = \sigma_{P_{\text{tot}}} \equiv \sigma$. Equation (23) then becomes:

$$\sigma^2_{m_{\text{miss}}} = \left(1 + 2\frac{P^2_{\text{tot}}}{m^2_{\text{miss}}} + 2\frac{P_{\text{tot}}\sqrt{P^2_{\text{tot}} + m^2_{\text{miss}}}}{m^2_{\text{miss}}}\right)\sigma^2$$

Reordering yields:

$$\sigma = \frac{\sigma_{m_{\text{miss}}}}{\sqrt{1 + 2\frac{P^2_{\text{tot}}}{m^2_{\text{miss}}} + 2\frac{P_{\text{tot}}\sqrt{P^2_{\text{tot}} + m^2_{\text{miss}}}}{m^2_{\text{miss}}}}} \tag{24}$$

Now $m_Z = 91.2$ GeV, so if we want to resolve this mass, the most we can have is $3\sigma_{m_{\text{miss}}} \approx m_Z$ in order for approximately the entire Z mass distribution to be positive. Hence, we need $\sigma_{m_{\text{miss}}} \approx \frac{m_Z}{3} = 30.4$ GeV. The smaller $\sigma_{m_{\text{miss}}}$ is, the better we can resolve m_Z.

Suppose:

1. $\sqrt{s} = 10$ TeV
2. $P_{\text{tot}} = \frac{\sqrt{s}}{2} = 5$ TeV
3. $\sigma_{E_{\text{tot}}} = \sigma_{P_{\text{tot}}} \equiv \sigma$
4. $\sigma_{m_{\text{miss}}} = 30.4$ GeV

Then, we can use equation (24) to determine the minimum resolution on E_{tot} and P_{tot} needed to resolve the Z mass:

$$\sigma \approx \frac{30.4}{\sqrt{1 + 2 \cdot \frac{5000^2}{91.2^2} + 2 \cdot \frac{5000 \cdot \sqrt{5000^2 + 91.2^2}}{91.2^2}}} \approx 0.2772 \text{ GeV}$$

This is the result for $\rho_{E_{\text{tot}},P_{\text{tot}}} = 1$, i.e. 100% correlation. Now, suppose E_{tot} and P_{tot} are independent, i.e. $\rho_{E_{\text{tot}},P_{\text{tot}}} = 0$. Along the same lines, we would find:

$$\sigma = \frac{\sigma_{m_{\text{miss}}}}{\sqrt{1 + 2\frac{P^2_{\text{tot}}}{m^2_{\text{miss}}}}} \approx \frac{30.4}{\sqrt{1 + 2 \cdot \frac{5000^2}{91.2^2}}} \approx 0.3921 \text{ GeV}$$

So, at a CM energy of 10 TeV, we need to have at most $\sigma \approx 0.2772$ GeV to be sure we can resolve the Z mass. The smaller σ is, the more accurately we can resolve m_Z.

Let us now find the actual value for $\sigma_{E_{\text{tot}}}$ ($\sigma_{P_{\text{tot}}}$) from the simulation data by plotting the difference between the total energy (total momentum) at generator level and the total energy (total momentum) at detector level. The standard deviations of these distributions are $\sigma_{E_{\text{tot,sim}}}$ and $\sigma_{P_{\text{tot,sim}}}$. See figure 25 for the results.

The σ_{sim} found in the simulation is three orders of magnitude larger than the maximum allowed σ that followed from the calculation. So, either not all particles are used at detector level, causing the large σ_{sim}, or the resolution of the detector becomes very low at this high CM energy of 10 TeV. The latter can be tested by running the same simulation at a lower CM energy, say $\sqrt{s} = 400$ GeV. Running through the calculation once more using $\sqrt{s} = 400$ GeV, we find that in order to be able to resolve the Z peak, the maximum allowed sigma is $\sigma \approx 6.604$ GeV. By making the same plots as in figure 25 for $\sqrt{s} = 400$ GeV, we obtain $\sigma_{\text{E}_{\text{tot,sim}}} = 27.8$ GeV and $\sigma_{\text{P}_{\text{tot,sim}}} = 22.8$ GeV. These

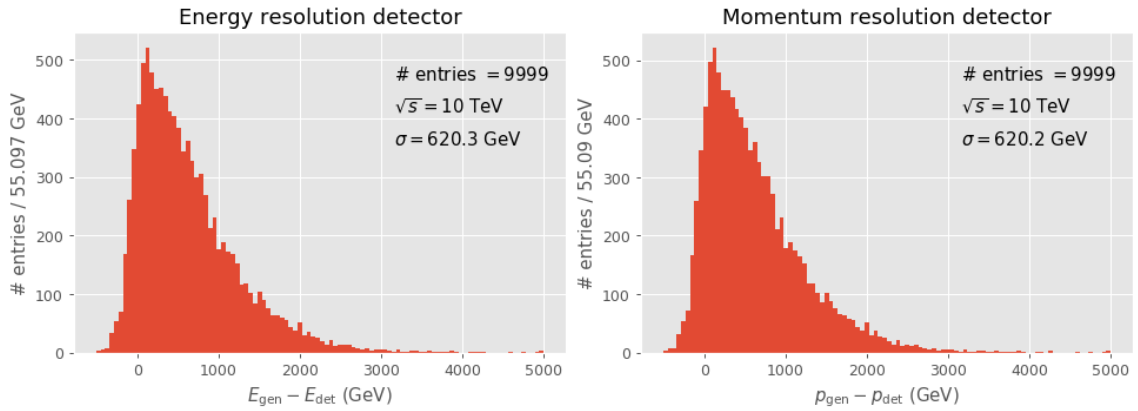

(a) (b)

Figure 25: *(a) Histogram of total energy at generator level minus the total energy at detector level. The distribution has a standard deviation* $\sigma = 620.3$ *GeV. (b) Histogram of total momentum at generator level minus the total momentum at detector level. The distribution has a standard deviation* $\sigma = 620.2$ *GeV. Both histograms show data for* $\sqrt{s} = 10$ *TeV.*

values are 'only' a factor four too large, which is much closer than the difference of three orders of magnitude obtained at $\sqrt{s} = 10$ TeV. Indeed, upon plotting the missing mass for the simulation at $\sqrt{s} = 400$ GeV, we get a reasonable peak near the Z mass (see figure 26). It overshoots the canonical value of 91.2 GeV slightly, which may be due to the detector resolution being four times too large, but could also be caused by some particles falling out of the jet reconstruction that actually do belong to the jets, thereby increasing the missing energy and decreasing the missing momentum, resulting in a greater missing mass.

It would seem that the low detector resolution is caused by the enormous 10 TeV CM energy. If this is indeed the case, it is highly necessary that research will be conducted towards the feasibility of the extremely high required resolution.

Not all particles detected or used in calculation The large missing mass distribution may be due to not all particles[31] being detected or taken into account in the calculations. Suppose neutrinos are the only particles that are not detected, then we can mimic the detector at generator level by leaving out the energies and momenta of all neutrinos. If indeed neutrinos are the only particles not being detected, we would expect that the distribution obtained by this method at generator level resembles the distribution obtained at detector level (figure 24). The result of the calculation of the missing mass at generator level with all neutrinos left out is shown in figure 27. Approximately two-thirds of all events have a missing mass above 100 GeV. This broad mass distribution resembles the distribution at detector level (figure 24). However, it is striking that we now see a clear peak around the Z mass in figure 27b. What is the difference between the events that have a proper reconstructed missing mass around 91 GeV and the events that have an inflated reconstructed missing mass?

Apparently, the events that have a proper missing mass have exactly two neutrinos (originating from the Z boson) whereas the events that have an inflated missing mass have more than two neutrinos. These extra neutrinos must originate from the jets of the Higgs boson[32]. Upon filtering out the events with extra neutrinos and plotting the result, we get a near-perfect missing mass distribution around the Z mass (see figure 28a). The missing mass distributions of the events with *more* than two neutrinos look very similar to the distribution we obtained at detector level, c.f. figures 28b and 24.

When extra neutrinos are created in the jets, they are not detected, which leads to an increase in missing energy. Along with this, there is a decrease in measured (and therefore missing) mo-

[31] Apart from the two neutrinos belonging to the Z boson.
[32] Since there are no other candidate particles in our process $\mu^+\mu^- \to Zh$, $Z \to \nu\overline{\nu}$, $h \to b\overline{b}$.

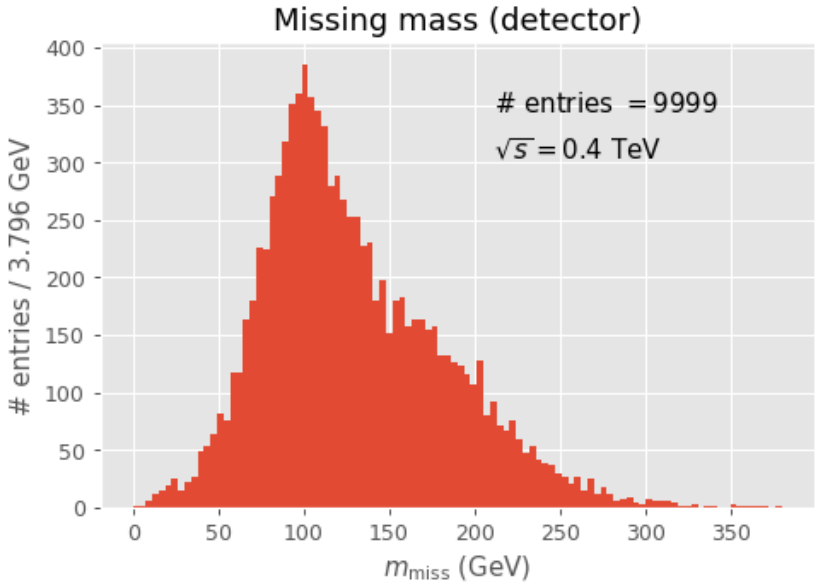

Figure 26: *Histogram of the missing invariant mass, calculated using particle-flows from* `Delphes`*;* $\sqrt{s} = 400$ *GeV.*

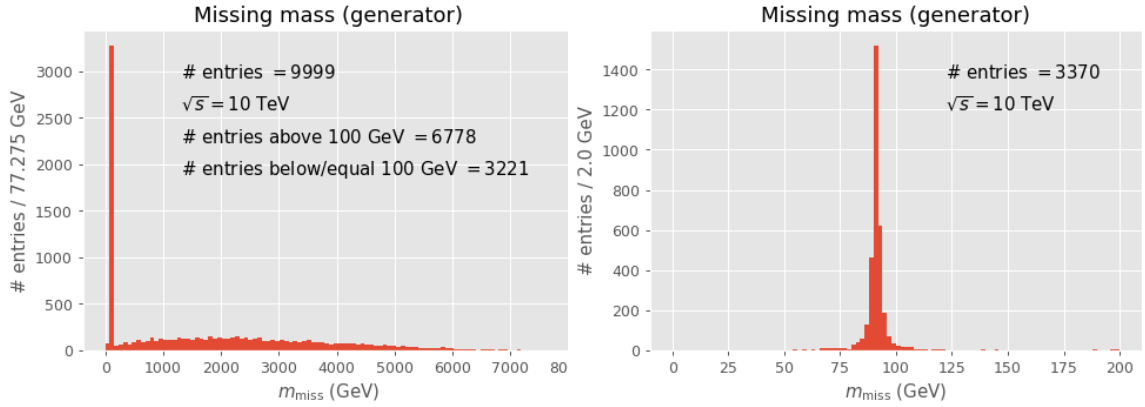

(a) (b)

Figure 27: *(a) Histogram of the missing invariant mass calculated at generator level while leaving out all neutrinos, thereby mimicking the detector. (b) Closeup of (a); the horizontal axis is limited to 200 GeV.*

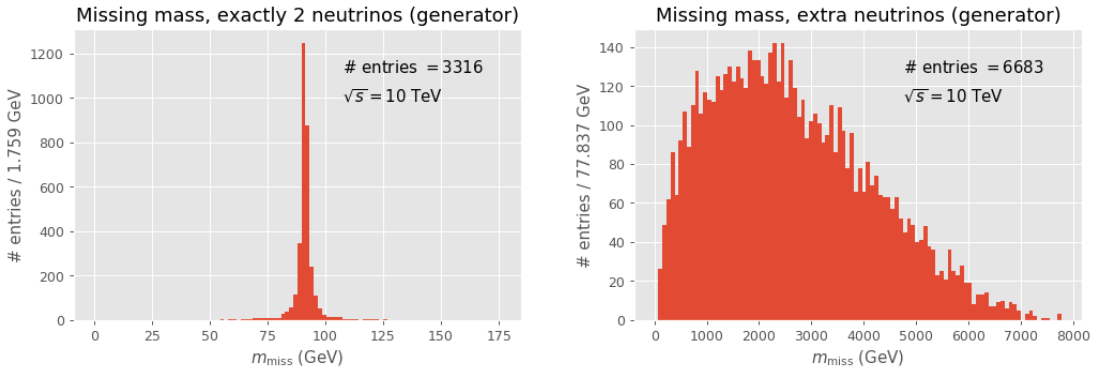

(a) (b)

Figure 28: *(a) Histogram of the missing invariant mass calculated at generator level while leaving out all neutrinos, thereby mimicking the detector. Only events with exactly two neutrinos are displayed. (b) Same as (a), but only showing events with more than two neutrinos.*

mentum. So, ultimately, we are left with a higher missing mass[33]. This explains why two-thirds of the events have a reconstructed mass that is too large. However, we still need an explanation for the peak around the Z mass at generator level (with all neutrinos left out) which is not present at detector level.

Figure 29 shows the mass distribution at detector level of the events that are in the Z peak at generator level. This looks remarkably similar to the original mass distribution at detector level (figure 24). Why are these missing masses so high? Let us have a look at the total energy, total momentum, missing energy and missing mass of five of these events, see table 3. Except for event 2, all the events in this table have E_{tot} and P_{tot} at detector level a few hundred GeV below those at generator level. Consequently, the missing mass shoots up. So, it seems that some particles are not used in the reconstruction at detector level that *are* used in the reconstruction at generator level.

A detector typically has muon chambers, i.e. trackers and calorimeters that are targeted towards the detection of muons. Muons typically do not leave many traces in the inner tracker (where electrons and positrons leave their traces) nor in the EM and hadronic calorimeters. Since the particle-flow algorithm, which is used for the calculation of the missing mass, is based on a combination of the information from the inner tracker and the EM and hadronic calorimeters, it could very well be that muons are not accounted for. Since the documentation of `Delphes` is rather limited to say the least, information about the muons could unfortunately not be located. Hence, it was not possible to further investigate the influence of muons on the missing mass distribution.

Another possibility as to why the detector observes fewer particles than there are at generator level, is an excessively high particle velocity or an inadequate detector resolution. Suppose two pions (π^-) formed as a result of Higgs decay, travel along directly adjacent paths. Because the pions have equal mass and charge, their radii of curvature in the tracker are identical. Consequently, if the resolution of the tracker is too low, the detector measures just a single path and, by mistake, reconstructs these two particles as just a single particle. The momentum reconstructed from this observation will therefore be too low. Now, because the particles travel at such high energies due to the aforementioned CM energy of 10 TeV, the curvature the particle paths undergo becomes very small; to the point of it even becoming difficult to distinguish adjacently traveling particles with different charges and masses. If this were in fact the case, the invariant mass of the two jets combined would turn out higher than the Higgs mass. However, we observed that the reconstructed mass of the jets is *lower* than the Higgs mass; see figure 15. It is therefore unlikely that the observation of fewer particles is due to the particles travelling sufficiently close that the detector reconstructs the momentum incorrectly.

[33]Note that this process might also contribute to the reconstructed Higgs mass being lower than 125 GeV (section 3.3), in addition to Bremsstrahlung of gluons and photons and an insufficient detector resolution.

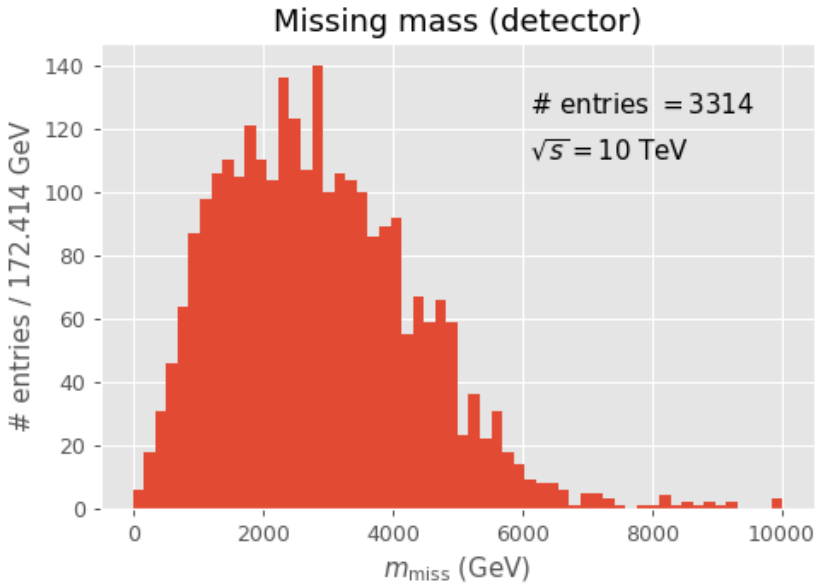

Figure 29: *Histogram of the missing invariant mass at detector level for the events that have a reconstructed missing mass around the canonical Z mass at generator level (while leaving out all neutrinos);* $\sqrt{s} = 10$ *TeV.*

		Generator (GeV)	**Detector (GeV)**
Event 2	E_{tot}	5000.497	5003.888
	P_{tot}	4998.934	5002.265
	Missing E	4999.503	4996.112
	Missing m	75.449	-1
Event 3	E_{tot}	5000.351	3959.213
	P_{tot}	4998.788	3957.777
	Missing E	4999.649	6040.787
	Missing m	92.768	4563.673
Event 6	E_{tot}	5000.351	4536.641
	P_{tot}	4998.788	4535.136
	Missing E	4999.649	5463.358
	Missing m	92.773	3046.444
Event 8	E_{tot}	5000.3657	4710.906
	P_{tot}	4998.802	4708.814
	Missing E	4999.635	5289.094
	Missing m	91.268	2408.648
Event 9	E_{tot}	5000.350	4554.853
	P_{tot}	4998.787	4553.237
	Missing E	4999.650	5445.148
	Missing m	92.900	2986.247

Table 3: *Five events that do have a reconstructed missing mass around the canonical Z mass at generator level, but do not at detector level. For each event, the total energy, the total momentum, the missing energy and the missing mass is displayed at both generator and detector level. All values are in GeV. The missing mass is set to -1 where* $P_{\text{tot}} > E_{\text{tot}}$.

4 Effects of Electroweak Bremsstrahlung

Let us have a look at the influence of EW Bremsstrahlung on the jet kinematics and (jet) reconstructions at the detector level. The simulation is repeated using the exact same events from `MadGraph 5`, but now EW Bremsstrahlung is turned on in `Pythia 8` (as explained in section 3.1). After discussing the direct implications on the generated interaction, the results are compared to those from the simulation without EW Bremsstrahlung. In addition, the effect of EW Bremsstrahlung on event-selections is investigated.

4.1 Branching modes

Since the switch for EW Bremsstrahlung is built into the `Pythia` part, the Higgs and Z boson directly originating from the muon-antimuon collision have the same kinematics as before. However, when EW showers are turned on, `Pythia` is allowed to overrule the decays $Z \to \nu\overline{\nu}$ and $h \to b\bar{b}$. Although in most cases the simulation will just follow the requested decays, the EW shower sometimes opts for a different interaction. For instance, the Higgs boson can act as a 'recoiler' by transferring momentum to the Z boson (the 'splitter') that consequently splits into a heavier particle-antiparticle pair, e.g. top-antitop (see figure 30). More information about this EW 'recoiler-splitter' mechanism can be found in reference [36].

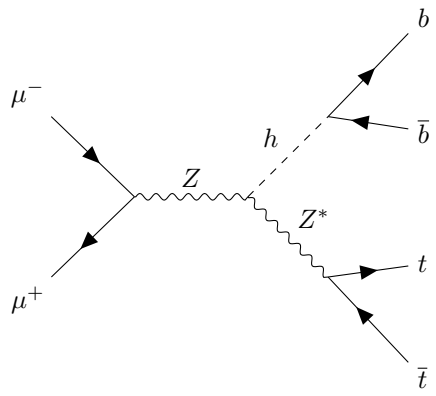

Figure 30: *Feynman diagram of a possible interaction due to EW effects in which the Higgs boson acts as a recoiler, enabling the Z boson to split into $t\bar{t}$. The star in Z^* indicates that the Z boson is brought off-shell.*

Figures 31 and 32 show the branching modes of the Higgs and Z bosons for all simulated events, for different CM energies. Clearly, the higher the CM energy, the larger the EW effects. At a CM energy of 10 TeV, 15.0% of the Z bosons split into W^+W^- rather than into neutral leptons, whereas this is only 7.5% at a CM energy of 3 TeV and even only 0.2% at 400 GeV. This result shows that the process $\mu^+\mu^- \to Zh$, where $Z \to \nu\overline{\nu}$ and $h \to b\bar{b}$ occurs less often than expected based on calculations using solely QCD and QED; EW effects need to be taken into account in order to properly determine the probability of the interaction. Most certainly, this goes for other processes as well.

4.2 Jet kinematics and multiplicities

The locations and momenta of the final-state particles for six events are plotted in figure 33. These are the same six events as plotted in figure 13, but this time with EW Bremsstrahlung turned on.

Event 5 (green) differs clearly for the simulations with and without EW Bremsstrahlung. In the left plot in figure 33, we see for this event three tight bunches of particles, indicating the presence of three jets, whereas the left plot in figure 13 shows only a single particle bunch. The other events do not show significant differences.

To get a quantitative feel for the influence of EW Bremsstrahlung, let us have a look at the jet multiplicities of all events using an inclusive jet reconstruction algorithm with $R = 0.2$ (as per sec-

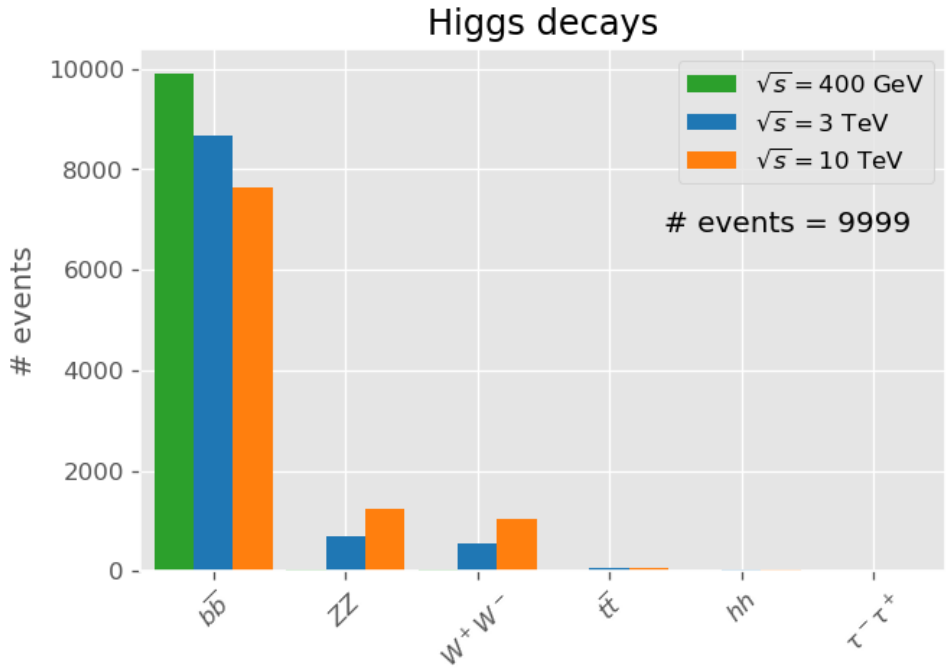

Figure 31: *Histogram of the branching modes of the initial Higgs boson in the simulation with EW Bremsstrahlung for different CM energies;* $\sqrt{s} = 400$ *GeV (green),* $\sqrt{s} = 3$ *TeV (blue) and* $\sqrt{s} = 10$ *TeV (orange).*

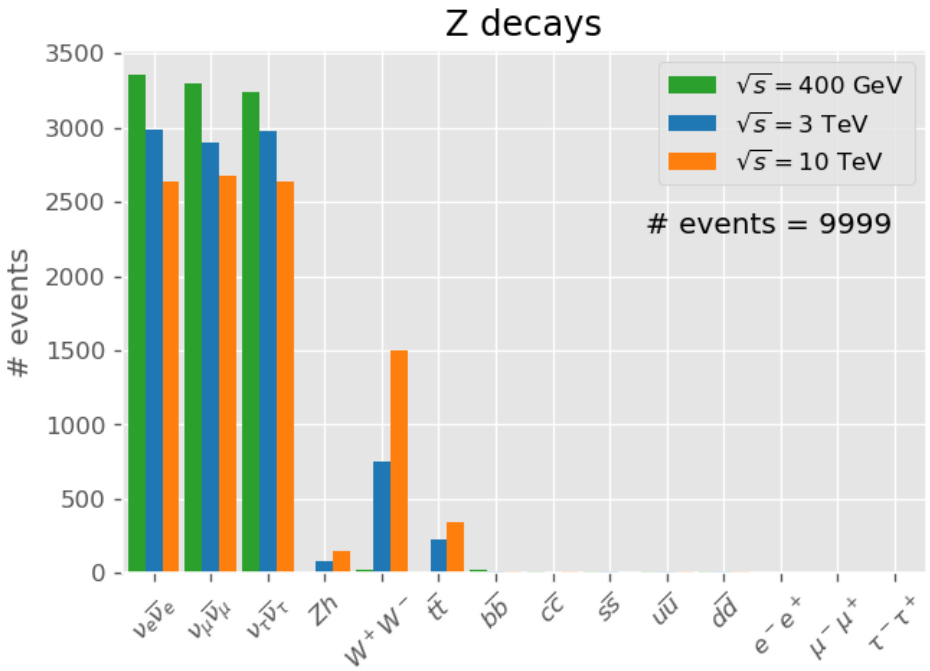

Figure 32: *Histogram of the branching modes of the initial Z boson in the simulation with EW Bremsstrahlung for different CM energies;* $\sqrt{s} = 400$ *GeV (green),* $\sqrt{s} = 3$ *TeV (blue) and* $\sqrt{s} = 10$ *TeV (orange).*

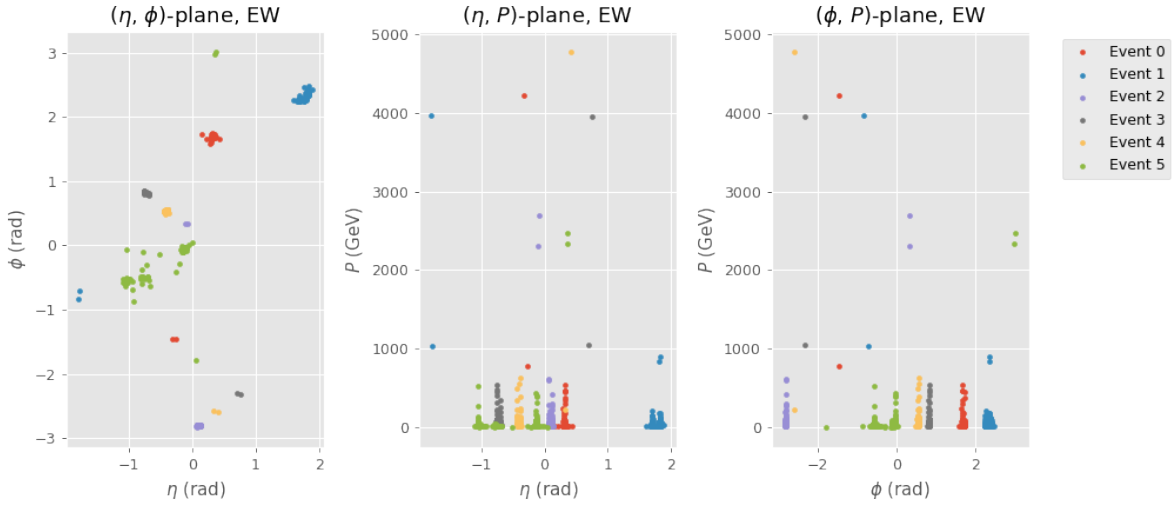

Figure 33: *Kinematics of the final-state particles in the generator, with EW Bremsstrahlung included. The first plot shows azimuthal angle ϕ against pseudorapidity η. The second and third plots show the total momentum P (in GeV) versus pseudorapidity η and azimuthal angle ϕ respectively.*

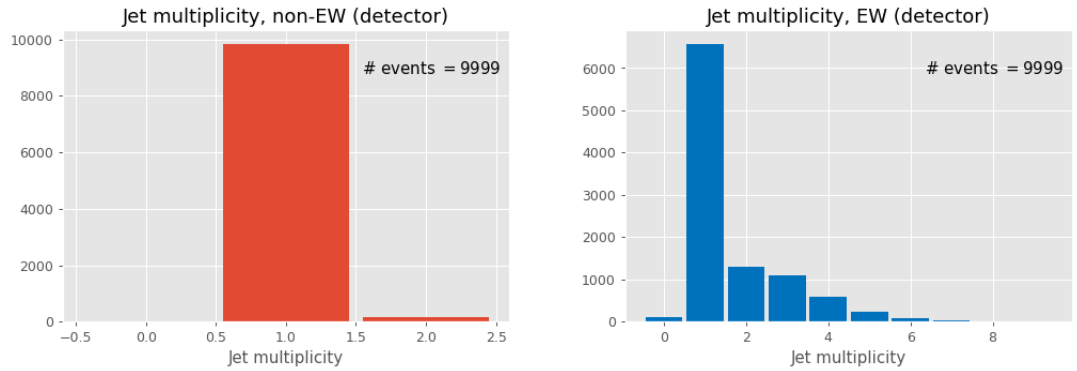

(a) (b)

Figure 34: *Histograms of jet multiplicities (i.e. number of jets) at the detector level found by an inclusive jet reconstruction algorithm, with $R = 0.2$. Figures (a) and (b) show the jet multiplicities for the simulations without and with EW Bremsstrahlung respectively; $\sqrt{s} = 10$ TeV.*

tion 3.2). Although most events still feature only a single reconstructed jet, the EW Bremsstrahlung causes a significant number of events to have more than one; see figure 34. These jet are of course a consequence of the different branching modes of the Z and Higgs (resulting from the EW effects). Consequently, selection procedures that select events with only two jets may miss many interesting events.

Looking at the jet multiplicities for the different Z branching modes (figure 35), we see that in almost all events that have only a single reconstructed jet $Z \to \nu\overline{\nu}$. Hence, a selection procedure based on the number of reconstructed jets might be a good way to select the events where $Z \to \nu\overline{\nu}$.

4.3 Reconstructing the Higgs and Z bosons

Higgs boson In section 3.3, the combined invariant mass of the two jets was found to be distributed according to figure 15. Along the same lines, we can find the combined mass of the jets for the new simulation with EW Bremsstrahlung included. Figure 36 shows the mass distribution for both, the simulation with EW Bremsstrahlung included (blue) and the simulation without EW Bremsstrahlung (red). They look similar; both feature peaks near 100 GeV and have approxi-

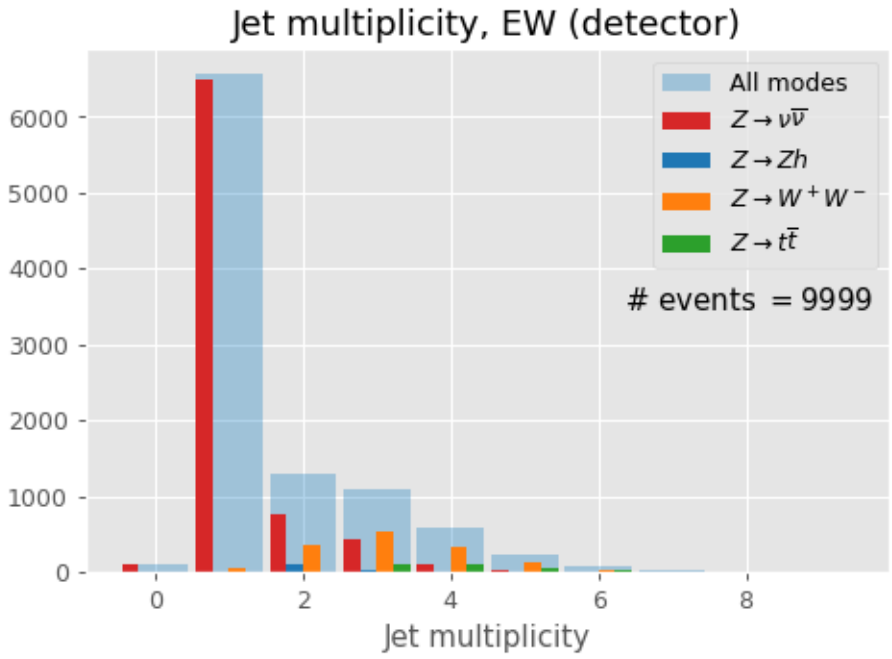

Figure 35: *Histogram of the jet multiplicities at detector level, found by an inclusive jet reconstruction algorithm, with $R = 0.2$. Each significant Z branching mode is plotted individually. The jet multiplicities for all modes together are plotted in half-transparent blue behind the individual branching modes.*

mately the same shape. However, the distribution with EW Bremsstrahlung included seems to be slightly shifted to the left and has a very long tail that reaches all the way to 10 TeV. The latter is due to the Z boson sometimes not decaying into neutral leptons. In the simulation without EW Bremsstrahlung, the tail does not extend beyond 183 GeV.

Z boson It was not possible to reconstruct the mass of the Z boson from the missing energy and missing momentum in the simulation without EW Bremsstrahlung (section 3.4). This may be due to the limited resolution of the detector in measuring E_{tot} and P_{tot}, or it may be that not all particles are accounted for in the calculation of E_{tot} and P_{tot}, or both could be the case. Since these aspects do not change upon inclusion of EW Bremsstrahlung into the simulation, and because the other branching modes of the Z boson invalidate the reconstruction method of missing momentum and missing energy, it is expected that proper reconstruction of the mass of the Z boson will remain yet impossible. Figure 37 shows that this is indeed the case.

4.4 Efficiency of event-selection procedures

In general, a simulation creates processes that one would like to find in a real particle collider. In practice, however, there may be other interactions that have very similar final states to the process of interest. These other interactions are known as 'background', and in order to study interactions in real life, they need to be filtered out. The exact event-selection procedure depends, of course, on the process to be investigated. Physical quantities that are often used in event-selection are transverse momentum P_T of specific particles or jets, pseudorapditiy η, difference in pseudorapditiy $|\Delta\eta|$ and mass m (see e.g. [39, 40, 41]). Furthermore, processes that contain jets often undergo a procedure named 'flavour tagging', in which an algorithm tries to determine the flavour of certain jet (i.e. whether it originates from e.g. a b-quark or a c-quark).

In our process, two jets originate from the b-quark and the $\bar{b}$-quark. The combined invariant mass of these jets is calculated, which should match the Higgs mass (section 3.3). It therefore makes sense to select events that have two b-tagged jets with a combined invariant mass near the

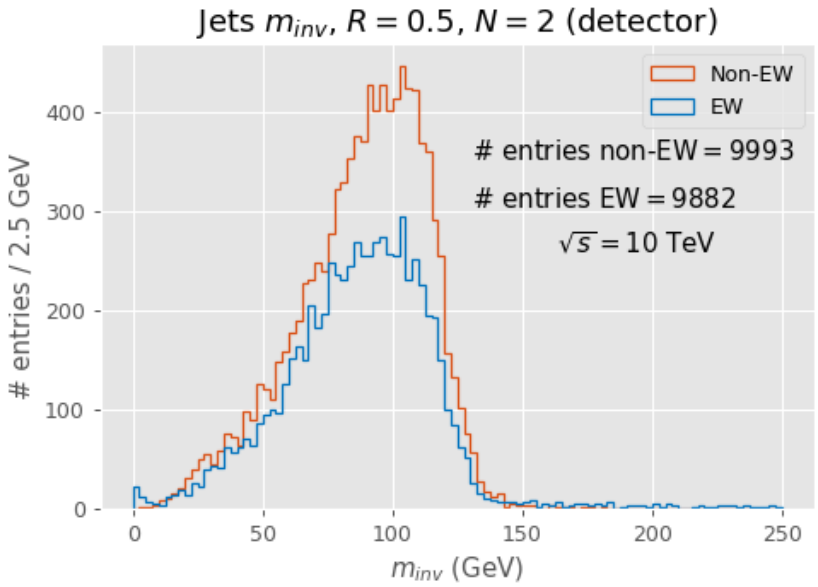

Figure 36: *Histogram of the invariant mass of the two jets into which the Higgs boson decays, simulated with EW Bremsstrahlung turned on (blue) and off (red). The jets are reconstructed using an exclusive jet clustering algorithm with $R = 0.5$. The blue histogram extends to 10 TeV, but for the sake of clarity the horizontal axis has been limited up to 250 GeV.*

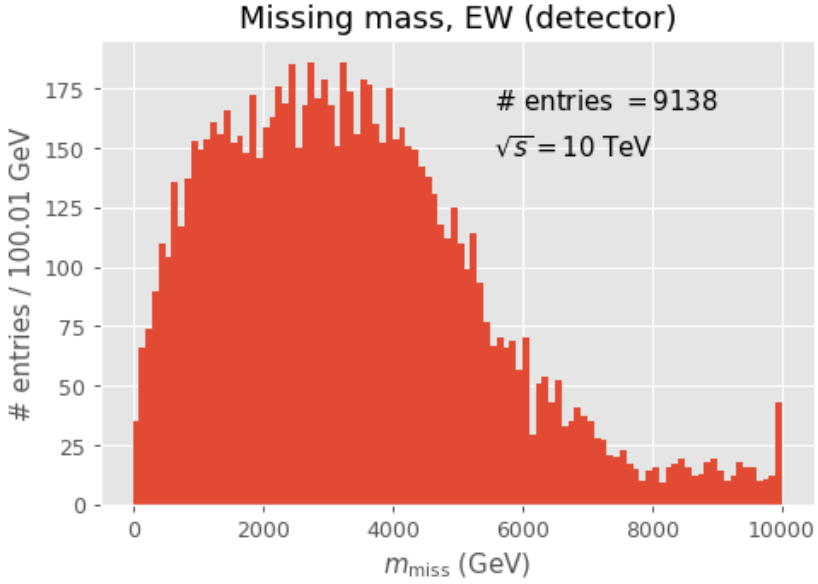

Figure 37: *Histogram of the missing invariant mass, calculated using particle-flows from* `Delphes` *for the simulation with EW Bremsstrahlung included; $\sqrt{s} = 10$ TeV.*

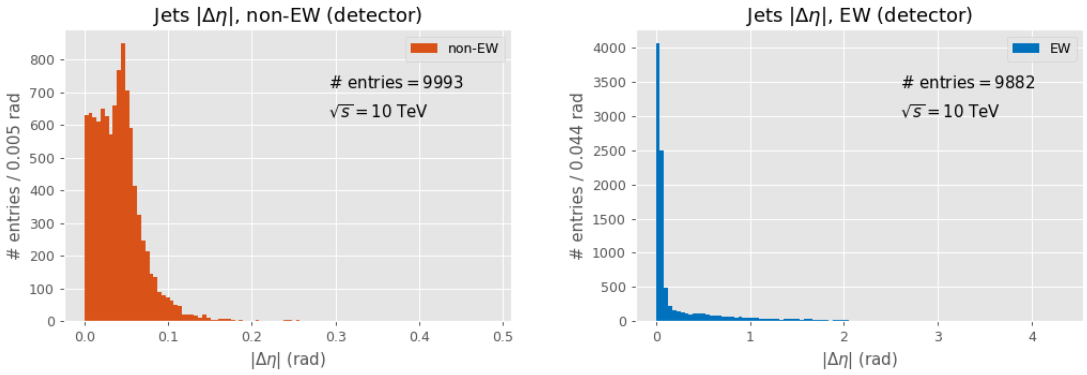

(a) (b)

Figure 38: *The absolute difference in pseudorapidity, $|\Delta\eta|$, between the two jets originating from the Higgs boson for the simulation without EW Bremsstrahlung (a) and with EW Bremsstrahlung included (b), $\sqrt{s} = 10$ TeV.*

Higgs mass of 125 GeV. In section 3.2, we observed that for a CM energy of 10 TeV, the jets are highly collimated due to the large Lorentz-boost of the Higgs boson. Hence, a selection based on the difference in pseudorapidity between the two jets is also possible. Let us find out how the inclusion of EW Bremsstrahlung into the simulation changes the efficiency of selection criteria on mass, $|\Delta\eta|$, b-tag and P_T.

Cut on Higgs mass Since both simulations have a reconstructed mass around 100 GeV (see figure 36), it is better to cut around 100 GeV instead of at the actual Higgs mass of 125 GeV. Applying the cut $|m_h - 100 \text{ GeV}| < 20$ GeV leaves 6064 out of 9993 events (i.e. 60.68%) in the simulation *without* EW Bremsstrahlung. Only 3845 out of 9882 events (i.e. 38.91%) survive the cut in the simulation *with* EW Bremsstrahlung. So, the inclusion of EW Bremsstrahlung causes a decrease of 21.77% in event-selection efficiency based on the combined mass of the two jets.

Jets close to each other Due to the high CM energy, the Higgs boson experiences a large Lorentz boost. Consequently, its two jets are highly collimated (see section 3.2). This feature can be exploited to filter the interesting events from background processes. The difference in pseudorapidity, $|\Delta\eta|$, for the simulation without and with EW Bremsstrahlung is shown in figures 38a and 38b respectively.

The figures show that the inclusion of EW Bremsstrahlung causes the reconstructed jets to have a larger $|\Delta\eta|$, which is due to the fact that more jets are created (c.f. figures 34a and 34b). The exclusive jet reconstruction algorithm does not always find the two b-jets; it can also return one b-jet and another jet caused by EW effects (e.g. Z splitting into W^+W^- or $t\bar{t}$), or perhaps even two jets caused by EW effects. The jets caused by the EW effects potentially form at larger angles to the original Higgs direction, resulting in larger $|\Delta\eta|$. Hence, when selecting events based on small differences in pseudorapidity, EW effects may cause many interesting events to be missed. Suppose we apply the cut $|\Delta\eta| < 0.2$, which seems reasonable based on figure 38a. This leaves 9959 out of 9993 events (i.e. 99.66%) in the simulation without EW Bremsstrahlung. However, upon the inclusion of EW Bremsstrahlung only 7355 out of 9882 events (i.e. 74.43%) remain after the cut. So, the inclusion of EW Bremsstrahlung causes a significant drop of 25.23% in event-selection efficiency based on difference in pseudorapidity between the two jets.

B-Tag As mentioned before, extra jets can be formed due to the inclusion of EW Bremsstrahlung. However, since a negligible amount of Z bosons split to $b\bar{b}$ (see figure 32), a nice way to work around this obstacle is to apply the requirement that two jets need to be b-tagged. The other selections (e.g. cuts on mass, $|\Delta\eta|$, P_T) can then be applied to these jets. In this case, it is crucial to use an

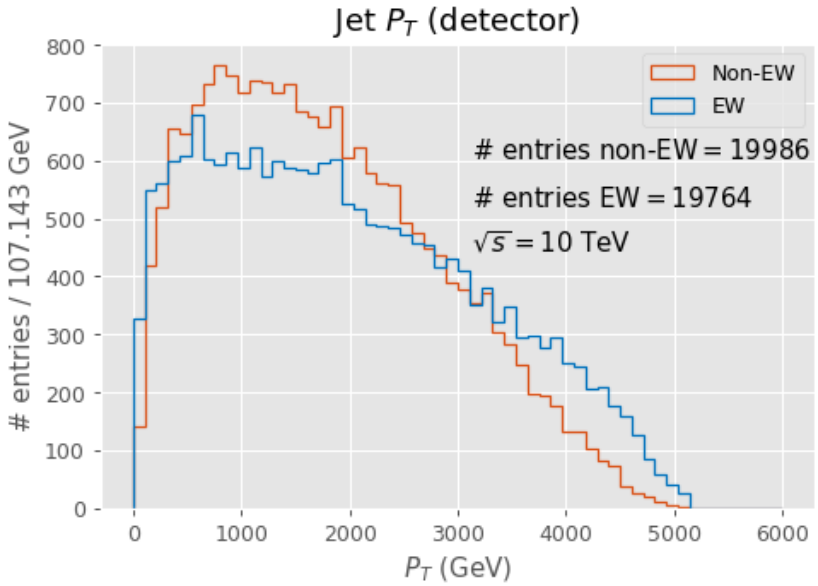

Figure 39: *Histogram of the transverse momentum of the two jets into which the Higgs boson decays, simulated with EW Bremsstrahlung turned on (blue) and off (red).*

inclusive jet reconstruction algorithm[34] so that, at the very least, the two b-jets are always found. In the simulations used in this thesis, the detector is, however, not able to resolve the two b-jets using an inclusive jet reconstruction algorithm for most events, since they are too collimated. Hence, the influence of EW Bremsstrahlung on the proposed b-tagging criterion cannot be investigated.

Cut on transverse momentum The transverse momentum P_T for the two simulations is distributed as in figure 39. Since this is a very broad distribution, a narrow cut should not be applied. Based on the simulation without EW Bremsstrahlung, the cut $P_T > 250$ GeV seems reasonable. Applying this cut to the simulation without EW Bremsstrahlung, 9257 out of 9993 events survive (i.e. 92.63%). Concerning the simulation with EW Bremsstrahlung, 8954 out of 9882 events (i.e. 90.61%) pass the cut. Because both distributions have a similar range and shape, we can only conclude that the effect of including EW Bremsstrahlung on the event-selection efficiency is small: a minor decrease of 2.02%.

[34] In an inclusive jet reconstruction algorithm, there is no restriction on the number of jets to be found, see section 2.4.

5 Conclusion

The two research questions that were investigated in this thesis are:

1. In a hypothetical Muon Collider operating at a centre of mass energy of 10 TeV, what is the influence of electroweak Bremsstrahlung on the efficiency of event-selection procedures concerning the process $\mu^+\mu^- \to Zh$, where $Z \to \nu\overline{\nu}$ and $h \to b\bar{b}$?
2. What difficulties, if any, occur in the Muon Collider Detector reconstruction of the process $\mu^+\mu^- \to Zh$, where $Z \to \nu\overline{\nu}$ and $h \to b\bar{b}$ at a centre of mass energy of 10 TeV?

The main effect of including EW Bremsstrahlung in the simulation of the process under investigation is that the decay $Z \to \nu\overline{\nu}$ occurs less often. The Higgs boson can transfer momentum to the Z boson, enabling the Z boson to split into a more massive particle-antiparticle and thereby start the formation of additional jets. The higher the CM energy, the more likely it is for the Z boson to interact in this way with the Higgs. E.g. at a CM energy of 10 TeV, 15.0% of the Z bosons split into W^+W^- rather than into neutral leptons, whereas this is only 7.5% at a CM energy of 3 TeV and even only 0.2% at 400 GeV. So, at the energies obtained in a Muon Collider, EW effects need to be taken into account to properly determine the probability of an interaction.

This formation of extra jets has a significant impact on event-selections based on the combined invariant mass of the jets and their differences in pseudorapidity; 21.77% fewer events pass the cut $|m_h - 100\text{ GeV}| < 20$ GeV due to the presence of EW effects. Furthermore, the inclusion of EW Bremsstrahlung causes 25.23% fewer events to pass the selection criterion $|\Delta\eta| < 0.2$. These obstacles may be eliminated by applying the requirement that two jets need to be b-tagged. To these two b-jets, the mass and $|\Delta\eta|$ cuts can then be applied. This way, jets due to EW effects are filtered out and only the relevant b-jets are used in subsequent selection criteria. Additionally, the influence of including EW Bremsstrahlung on an event-selection based on transverse momentum, $P_T > 250$ GeV, is minor. Only 2.02% fewer events pass this selection due to EW Bremsstrahlung.

Difficulties were found in the reconstruction of the process $\mu^+\mu^- \to Zh$, where $Z \to \nu\overline{\nu}$ and $h \to b\bar{b}$ at a CM energy of 10 TeV. Firstly, the Lorentz boost that the Higgs boson obtains due to this large CM energy causes its decay products, i.e. the jets, to be highly collimated. Consequently, the Valencia inclusive jet reconstruction algorithm is not able to properly distinguish the two jets and rather reconstructs them as a single jet. This is important when selecting events based on their number of jets.

Secondly, the combined invariant mass of the two reconstructed jets, obtained using exclusive clustering, is approximately 25 GeV smaller than the canonical Higgs mass of 125 GeV. The main cause remains unclear, although it is within the realm of possibility that the high particle energies cause the detector to be unable to detect all particles. Causes that have been excluded are Bremsstrahlung of photons and gluons, and the usage of an insufficiently large jet-size parameter R in the jet reconstruction.

Thirdly, the mass of the Z boson, 91 GeV, could not be properly reconstructed by means of missing energy and missing momentum; the resulting missing mass distribution extends over several thousands of GeV and peaks at 4000 GeV. Multiple possible causes were investigated, and it can certainly be excluded that this strange distribution is due to particles escaping through the beam openings. On the other hand, a significant factor is the creation of (anti)neutrinos in the jets originating from the Higgs boson. Furthermore, the detector resolution plays an important role; at the CM energy of 10 TeV, the detector has an insufficient resolution, thereby losing the ability to measure the total energy and total momentum with acceptable accuracy. The resulting uncertainty on said measurements causes the missing mass distribution to be far from the distribution of the actual Z mass.

6 Discussion and Outlook

The research conducted in this thesis is merely an introductory exploration into the effects of the energy regime that can be obtained by a Muon Collider. Nonetheless, numerous obstacles have been found that demand serious further investigation.

In the process $\mu^+\mu^- \to Zh$, where $Z \to \nu\overline{\nu}$ and $h \to b\bar{b}$ at a CM energy of 10 TeV, the Higgs boson is significantly boosted, resulting in highly collimated b-jets. Consequently, the Valencia inclusive jet reconstruction algorithm used is not able to properly distinguish the two jets. In order to better reconstruct the Higgs mass in the $h \to b\bar{b}$ decay, it would be good to investigate the effects of a smaller R in the Valencia reconstruction algorithm; R is currently limited to a minimum of 0.2 in the inclusive algorithm. It is also possible to accept the fact that the two jets are reconstructed as a single jet and adapt the event-selection procedures accordingly. Furthermore, investigation into other reconstruction algorithms is recommended. The Delphes card (see reference [38]) includes nine different jet reconstruction algorithms, a.o. SIScone, kt, Cambridge/Aachen and anti-kt. Other algorithms than Valencia might be better in distinguishing the boosted jets.

A real bottleneck appears to be that large uncertainties on the detector measurements of total energy and total momentum arise due to the enormous CM energy. Consequently, mass reconstruction of the Z boson decaying to neutral leptons by means of missing energy and missing momentum, becomes a challenging task. Needless to say, it is highly necessary that research is conducted in order to rise to the challenge of this extremely high detector resolution.

EW Bremsstrahlung has been found to have a significant effect on the efficiency of event-selection procedures. However, in this thesis no background processes were considered. The cuts have been solely based on the actual signal $h \to b\bar{b}$. In reality, cuts are determined from both the signal and background processes. Since $h \to b\bar{b}$ has a notoriously large background, it is important that further research will be conducted towards the effects of EW Bremsstrahlung on event-selection procedures, taking background processes into account. Because of the enormous branching ratio of $h \to b\bar{b}$, it would be very interesting if the Higgs can be reconstructed through this decay channel. To that end, using a more detailed simulation of the Muon Collider Detector, it is necessary that an optimal selection-procedure is constructed targeted towards the reconstruction of the Higgs mass through its decay into a bottom-antibottom pair, while considering relevant background processes and EW effects.

A serious limitation that affected this thesis was the incredibly limited documentation regarding `Delphes`. Consequently, assumptions had to be made about the meaning of some quantities in the `Delphes` data set. E.g., the mass returned by the Valencia reconstruction algorithm had strangely low values, however, it has been assumed that this mass is the invariant mass of the reconstructed jets. Beyond this, there is little information about the particle-flow data sets. It has been assumed that these data sets contain all information about the detected particles, but the results show that many particles are missing. The limited documentation makes it difficult to draw strong conclusions. For further research into effects due to the energy regime of the Muon Collider, it is recommended that either the `Delphes` community is approached in order to obtain better documentation, or different, better-documented, detector simulation software is used.

Bibliography

[1] MissMJ, Cush. *Standard Model of Elementary Particles*. 2019. URL: https://commons.wikimedia.org/wiki/File:Standard_Model_of_Elementary_Particles.svg (visited on 05/14/2021).

[2] David J. Griffiths. *Introduction to elementary particles*. Wiley, 1987.

[3] G. Gabrielse et al. "Towards an Improved Test of the Standard Model's Most Precise Prediction". In: *Atoms* 7.2 (2019), p. 45. DOI: 10.3390/atoms7020045. arXiv: 1904.06174 [quant-ph].

[4] Vardan Khachatryan et al. "Precise determination of the mass of the Higgs boson and tests of compatibility of its couplings with the standard model predictions using proton collisions at 7 and 8 TeV". In: *Eur. Phys. J. C* 75.5 (2015), p. 212. DOI: 10.1140/epjc/s10052-015-3351-7. arXiv: 1412.8662 [hep-ex].

[5] J. Breitweg et al. "Comparison of ZEUS data with standard model predictions for $e^+p \to e^+X$ scattering at high x and Q^2". In: *Z. Phys. C* 74 (1997), pp. 207–220. DOI: 10.1007/s002880050384. arXiv: hep-ex/9702015.

[6] Richard Massey, Thomas Kitching, and Johan Richard. "The dark matter of gravitational lensing". In: *Reports on Progress in Physics* 73.8 (July 2010), p. 086901. ISSN: 1361-6633. DOI: 10.1088/0034-4885/73/8/086901. URL: http://dx.doi.org/10.1088/0034-4885/73/8/086901.

[7] Hitoshi Murayama. *Physics Beyond the Standard Model and Dark Matter*. 2007. arXiv: 0704.2276 [hep-ph].

[8] Sveva Castello, Stéphane Ilić, and Martin Kunz. "An updated dark energy view of inflation". In: (Apr. 2021). arXiv: 2104.15091 [astro-ph.CO].

[9] CERN. *The matter-antimatter asymmetry problem*. 2021. URL: https://home.cern/science/physics/matter-antimatter-asymmetry-problem (visited on 05/13/2021).

[10] Maximilien Brice (CERN). *Aerial View of the CERN*. 2008. URL: https://commons.wikimedia.org/wiki/File:CERN_Aerial_View.jpg (visited on 05/14/2021).

[11] CERN. *LHC the guide*. 2017. URL: https://home.cern/sites/home.web.cern.ch/files/2018-07/CERN-Brochure-2017-002-Eng_0.pdf (visited on 05/14/2021).

[12] Carlos. *ATLAS (A Toroidal LHC ApparatuS)*. 2008. URL: http://lahoracero.org/atlas-a-toroidal-lhc-apparatus/ (visited on 07/18/2021).

[13] Riccardo Maria Bianchi. "Higgs candidate decaying to 2 tau leptons in the ATLAS detector". In: (Nov. 2013). General Photo. URL: https://cds.cern.ch/record/1631395.

[14] Georges Aad et al. "Observation of a new particle in the search for the Standard Model Higgs boson with the ATLAS detector at the LHC". In: *Phys. Lett. B* 716 (2012), pp. 1–29. DOI: 10.1016/j.physletb.2012.08.020. arXiv: 1207.7214 [hep-ex].

[15] Serguei Chatrchyan et al. "Observation of a New Boson at a Mass of 125 GeV with the CMS Experiment at the LHC". In: *Phys. Lett. B* 716 (2012), pp. 30–61. DOI: 10.1016/j.physletb.2012.08.021. arXiv: 1207.7235 [hep-ex].

[16] Manuela Boscolo, Jean-Pierre Delahaye, and Mark Palmer. "The Future Prospects of Muon Colliders and Neutrino Factories". In: *Reviews of Accelerator Science and Technology* (Sept. 2019), pp. 189–214. DOI: 10.1142/9789811209604_0010. URL: http://dx.doi.org/10.1142/9789811209604_0010.

[17] Jean Pierre Delahaye et al. *Muon Colliders*. 2019. arXiv: 1901.06150 [physics.acc-ph].

[18] Tadeusz Lesiak. "The day after LHC: electron-positron colliders are marching on". In: *Proc. SPIE Int. Soc. Opt. Eng.* 11054 (2019). Ed. by Dariusz Bocian and Ryszard S. Romaniuk, p. 1105404. DOI: 10.1117/12.2524110.

[19] Vladimir Shiltsev. "Considerations On Energy Frontier Colliders After LHC". In: *2nd North American Particle Accelerator Conference*. Jan. 2017. DOI: 10.18429/JACoW-NAPAC2016-TUPOB07. arXiv: 1705.02011 [physics.acc-ph].

[20] Nazar Bartosik et al. "Muon collider: the Low EMittance Muon Accelerator (LEMMA) approach". In: *PoS* LeptonPhoton2019 (2019), p. 047. DOI: 10.22323/1.367.0047.

[21] Frank Zimmermann. "Future colliders for particle physics —"Big and small"". In: *Nucl. Instrum. Meth. A* 909 (2018), pp. 33–37. DOI: 10.1016/j.nima.2018.01.034. arXiv: 1801.03170 [physics.acc-ph].

[22] Klauw Wille. *Synchrotron Radiation*. 2013. URL: https://indico.cern.ch/event/218284/contributions/1520454/attachments/352184/490697/JUAS2013_Synchrotron_Radiation_1.pdf (visited on 05/18/2021).

[23] P. A. Zyla et al. "Review of Particle Physics". In: *PTEP* 2020.8 (2020), p. 083C01. DOI: 10.1093/ptep/ptaa104.

[24] Lorenzo Sestini et al. "Higgs physics possibilities at a Muon Collider". In: *PoS* ICHEP2020 (2021), p. 083. DOI: 10.22323/1.390.0083.

[25] Roberto Franceschini and Mario Greco. "Higgs and BSM Physics at the future Muon Collider". In: (Apr. 2021). arXiv: 2104.05770 [hep-ph].

[26] CMS Collaboration. *The two most massive quarks put the spotlight on the Higgs boson*. 2019. URL: https://cms.cern/news/two-most-massive-quarks-put-spotlight-higgs-boson (visited on 05/19/2021).

[27] Ryan Atkin. "Review of jet reconstruction algorithms". In: *J. Phys. Conf. Ser.* 645.1 (2015). Ed. by Alan S. Cornell and Bruce Mellado, p. 012008. DOI: 10.1088/1742-6596/645/1/012008.

[28] Março Boronat et al. "A robust jet reconstruction algorithm for high-energy lepton colliders". In: *Phys. Lett. B* 750 (2015), pp. 95–99. DOI: 10.1016/j.physletb.2015.08.055. arXiv: 1404.4294 [hep-ex].

[29] M. Boronat et al. "Jet reconstruction at high-energy electron–positron colliders". In: *Eur. Phys. J. C* 78.2 (2018), p. 144. DOI: 10.1140/epjc/s10052-018-5594-6. arXiv: 1607.05039 [hep-ex].

[30] Dr Sachintha Hapugoda. *Bremsstrahlung radiation (diagram)*. URL: https://radiopaedia.org/cases/bremsstrahlung-radiation-diagram-2 (visited on 06/06/2021).

[31] A. D. Martin et al. "Parton distributions for the LHC". In: *Eur. Phys. J. C* 63 (2009), pp. 189–285. DOI: 10.1140/epjc/s10052-009-1072-5. arXiv: 0901.0002 [hep-ph].

[32] Sofia Maria Consonni. "Higgs search at ATLAS". In: *International School on High Energy Physics: Workshop on High Energy Physics in the near Future*. May 2013. arXiv: 1305.3315 [hep-ex].

[33] S. Dittmaier et al. "Handbook of LHC Higgs Cross Sections: 1. Inclusive Observables". In: (Jan. 2011). DOI: 10.5170/CERN-2011-002. arXiv: 1101.0593 [hep-ph].

[34] J. Alwall et al. "The automated computation of tree-level and next-to-leading order differential cross sections, and their matching to parton shower simulations". In: *Journal of High Energy Physics* 2014.7 (July 2014). ISSN: 1029-8479. DOI: 10.1007/jhep07(2014)079. URL: http://dx.doi.org/10.1007/JHEP07(2014)079.

[35] Pythia 8 community. *VINCIA QED and EW Antenna Shower Settings*. URL: https://pythia.org/manuals/pythia8305/Welcome.html (visited on 06/06/2021).

[36] R. J. Verheyen. "Electroweak Effects in Antenna Parton Showers". PhD thesis. Radboud University Nijmegen, 2020.

[37] J. de Favereau et al. "DELPHES 3: a modular framework for fast simulation of a generic collider experiment". In: *Journal of High Energy Physics* 2014.2 (Feb. 2014). ISSN: 1029-8479. DOI: 10.1007/jhep02(2014)057. URL: http://dx.doi.org/10.1007/JHEP02(2014)057.

[38] Michele Selvaggi, Ulrike Schnoor. *Muon Collider Detector TARGET model*. URL: https://github.com/delphes/delphes/blob/master/cards/delphes_card_MuonColliderDet.tcl (visited on 06/06/2021).

[39] Georges Aad et al. "Search for new phenomena with top quark pairs in final states with one lepton, jets, and missing transverse momentum in pp collisions at $\sqrt{s} = 13$ TeV with the ATLAS detector". In: *JHEP* 04 (2021), p. 174. DOI: 10.1007/JHEP04(2021)174. arXiv: 2012.03799 [hep-ex].

[40] A. M. Sirunyan et al. "Search for a massive resonance decaying to a pair of Higgs bosons in the four b quark final state in proton-proton collisions at $\sqrt{s} = 13$ TeV". In: *Phys. Lett. B* 781 (2018), pp. 244–269. DOI: 10.1016/j.physletb.2018.03.084. arXiv: 1710.04960 [hep-ex].

[41] Albert M. Sirunyan et al. "Search for resonant pair production of Higgs bosons decaying to bottom quark-antiquark pairs in proton-proton collisions at 13 TeV". In: *JHEP* 08 (2018), p. 152. DOI: 10.1007/JHEP08(2018)152. arXiv: 1806.03548 [hep-ex].

Appendix A Choosing the Interaction

It would be interesting to investigate the phenomenon of Higgs self-coupling, e.g. in $\mu^+\mu^- \to Zhh$. However, in order for this thesis to be interesting for the Muon Collider, the process being investigated must occur often enough in the Muon Collider. Otherwise, the process would occur so rarely, that it does not matter whether EW Bremsstrahlung has an effect since the statistics are too insignificant to justify investigation of the process. Therefore, for different processes, the number of expected events at the Muon Collider operating at a centre of mass energy of 10 TeV are calculated. A lifetime of five years is assumed, so that we have an integrated luminosity of 10 ab^{-1} [17].

Given the cross section of the interaction (σ) together with the integrated luminosity of a particle collider ($\mathcal{L}_{\text{int}}$), the expected number of events can easily be calculated using equation (25):

$$N = \mathcal{L}_{\text{int}} \cdot \sigma \tag{25}$$

The cross sections for the different interactions are determined using `MadGraph 5`. The results are laid out in table 4.

Interaction	$\sigma\,(\text{pb}^{-1})$	N
$\mu^+\mu^- \to Zhh$, $Z \to e^+e^-$, $h \to b\bar{b}$, $h \to b\bar{b}$	$1.400 \cdot 10^{-7}$	1.4
$\mu^+\mu^- \to Zhh$, $Z \to \nu\overline{\nu}$, $h \to b\bar{b}$, $h \to b\bar{b}$	$8.270 \cdot 10^{-7}$	8.3
$\mu^+\mu^- \to Zhh$, $Z \to l\bar{l}$, $h \to q\bar{q}$, $h \to q\bar{q}$	$1.248 \cdot 10^{-6}$	12.5
$\mu^+\mu^- \to Zh$, $Z \to \nu\overline{\nu}$, $h \to b\bar{b}$	$2.030 \cdot 10^{-5}$	203.0

Table 4: *The expected number of events (N) for different interactions in the Muon Collider operating at $\sqrt{s} = 10$ TeV with $\mathcal{L}_{\text{int}} = 10\ \text{ab}^{-1}$. N is calculated using the cross section (σ) determined by* ***`MadGraph 5`****.*

Appendix B Effect of Lorentz Boost on Jets

The effect of the large Lorentz boost of the Higgs boson on the two jets into which it decays can be investigated by means of a Monte Carlo simulation.

First, we define the following values:

$$\begin{aligned} m_h &= 125.0 \text{ GeV} \\ m_Z &= 91.2 \text{ GeV} \\ m_b &= 4.2 \text{ GeV} \end{aligned}$$

We leave the squared CM energy, s, undefined so that the effect can be investigated for different CM energies and thus for different boosts. Next, we calculate the energy and momentum of the Higgs boson along with its Lorentz factor γ and its velocity relative to the speed of light β:

$$\begin{aligned} E_h &= \frac{s + m_h^2 - m_Z^2}{2\sqrt{s}} \\ p_h &= \sqrt{E_h^2 - m_h^2} \\ \gamma_h &= \frac{E_h}{m_h} \\ \beta_h &= \frac{p_h}{E_h} \end{aligned}$$

Next, we draw a random four-momentum for the b-quark in the rest frame of the Higgs boson. To that end, we set the energy of the b-quark to half the Higgs mass[35] and calculate its momentum:

$$E_b = \frac{m_h}{2}$$
$$p_b = \sqrt{E_b^2 - m_b^2}$$

Then, we draw a random polar angle θ from the interval $[0, \pi]$ and an azimuthal angle ϕ from $[0, 2\pi]$:

$$\theta = \mathcal{R} \cdot \pi$$
$$\phi = \mathcal{R} \cdot 2\pi$$

This determines the four-momentum of the b-quark:

$$p_b^\mu = (E_b, \quad p_b \sin\theta\cos\phi, \quad p_b \sin\theta\sin\phi, \quad p_b\cos\theta)^{\mathrm{T}}$$

where the T indicates a transpose; making it a column vector rather than a row vector. Now, we boost the system to the lab frame:

$$q_b^\mu = \begin{pmatrix} \gamma_h & 0 & 0 & \beta_h\gamma_h \\ 0 & 1 & 0 & 0 \\ 0 & 0 & 1 & 0 \\ \beta_h\gamma_h & 0 & 0 & \gamma_h \end{pmatrix} \begin{pmatrix} E_b \\ p_b\sin\theta\cos\phi \\ p_b\sin\theta\sin\phi \\ p_b\cos\theta \end{pmatrix} = \begin{pmatrix} \gamma_h\left(E_b + \beta_h p_b\cos\theta\right) \\ p_b\sin\theta\cos\phi \\ p_b\sin\theta\sin\phi \\ \gamma_h\left(p_b\cos\theta + \beta_h E_b\right) \end{pmatrix}$$

Since the total energy and momentum of the Higgs boson need to be conserved, we automatically obtain the four-momentum of the $\bar{b}$-quark:

$$q_{\bar{b}}^\mu = \begin{pmatrix} E_h - \gamma_h\left(E_b + \beta_h p_b\cos\theta\right) \\ -p_b\sin\theta\cos\phi \\ -p_b\sin\theta\sin\phi \\ p_h - \gamma_h\left(p_b\cos\theta + \beta_h E_b\right) \end{pmatrix}$$

The next step is to exploit the definition of the inner product of three-vectors to calculate the angle α between the two quarks, i.e. the angle between the two jets, in the lab frame:

$$\boldsymbol{q_b} \cdot \boldsymbol{q_{\bar{b}}} = |\boldsymbol{q_b}|\,|\boldsymbol{q_{\bar{b}}}|\cos\alpha$$

$$\alpha = \arccos\left(\frac{\boldsymbol{q_b} \cdot \boldsymbol{q_{\bar{b}}}}{|\boldsymbol{q_b}|\,|\boldsymbol{q_{\bar{b}}}|}\right)$$

Executing this procedure 1,000,000 times for different $\sqrt{s}$ results in the histogram in figure 40. Indeed, the jets become extremely collimated due to the Lorentz boost of the Higgs boson at a CM energy of 10 TeV.

[35] This is the energy of the b-quark in the rest frame of the Higgs. It must therefore be equal to half the Higgs mass.

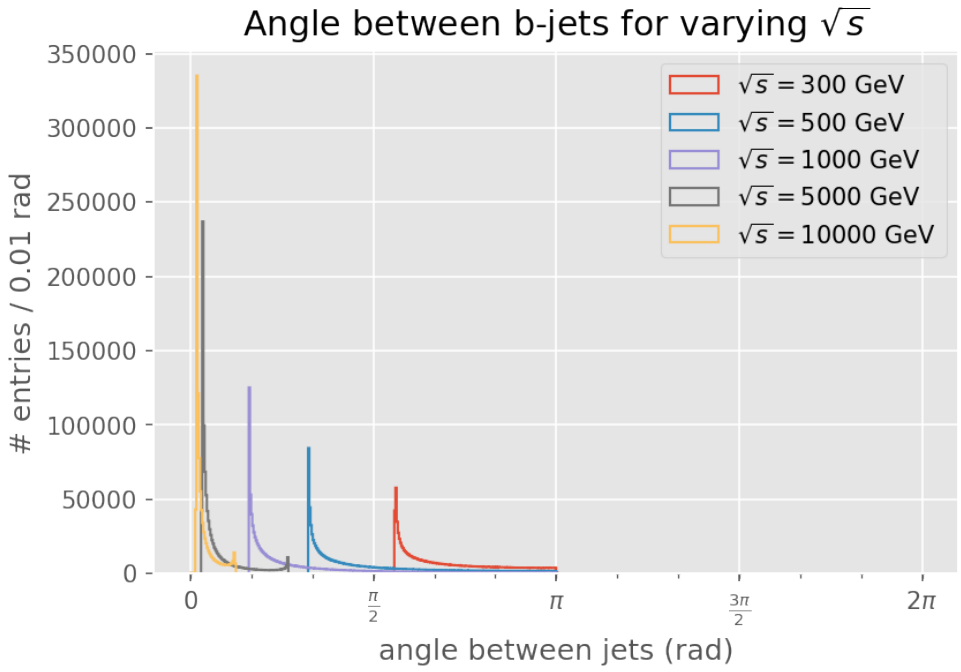

Figure 40: *Histogram of the angle (in radians) between the two jets originating from the Higgs boson for different CM energies.*

Appendix C Python Code

The data from the simulations is extracted and analysed using the programming language `Python`. If interested, the reader can obtain the code used for the analysis via e-mail, *Bob.Truijen@student.ru.nl*.